

# Mixed Policy Gradient

Yang Guan<sup>1</sup>, Jingliang Duan<sup>1</sup>, Shengbo Eben Li<sup>1</sup>, Jie Li<sup>1</sup>, Jianyu Chen<sup>2</sup>, Bo Cheng<sup>1</sup>

**Abstract**—Reinforcement learning (RL) has great potential in sequential decision-making. At present, the mainstream RL algorithms are data-driven, relying on millions of iterations and a large number of empirical data to learn a policy. Although data-driven RL may have excellent asymptotic performance, it usually yields slow convergence speed. As a comparison, model-driven RL employs a differentiable transition model to improve convergence speed, in which the policy gradient (PG) is calculated by using the backpropagation through time (BPTT) technique. However, such methods suffer from numerical instability, model error sensitivity and low computing efficiency, which may lead to poor policies. In this paper, a mixed policy gradient (MPG) method is proposed, which uses both empirical data and the transition model to construct the PG, so as to accelerate the convergence speed without losing the optimality guarantee. MPG contains two types of PG: 1) data-driven PG, which is obtained by directly calculating the derivative of the learned Q-value function with respect to actions, and 2) model-driven PG, which is calculated using BPTT based on the model-predictive return. We unify them by revealing the correlation between the upper bound of the unified PG error and the predictive horizon, where the data-driven PG is regarded as 0-step model-predictive return. Relying on that, MPG employs a rule-based method to adaptively adjust the weights of data-driven and model-driven PGs. In particular, to get a more accurate PG, the weight of the data-driven PG is designed to grow along the learning process while the other to decrease. Besides, an asynchronous learning framework is proposed to reduce the wall-clock time needed for each update iteration. Simulation results show that the MPG method achieves the best asymptotic performance and convergence speed compared with other baseline algorithms.

**Index Terms**—Reinforcement Learning, Policy Gradient, Model-free RL, Model-based RL.

## I. INTRODUCTION

Reinforcement learning (RL) algorithms have been applied in a wide variety of challenging domains and achieved good performance, ranging from games to robotic control [1]–[4]. Policy gradient (PG) is one of the main categories of RL and has drawn great attention due to its suitability for continuous action space and deterministic policy. PG methods can be categorized into data-driven methods and model-driven methods. The former learns a policy purely from empirical data generated by interaction between the agent and a environment or high-fidelity simulators, whereas the latter learns through backpropagation through time (BPTT) with the help of transition models.

This work was supported by International Science & Technology Cooperation Program of China under 2019YFE0100200, Tsinghua University-Toyota Joint Research Center for AI Technology of Automated Vehicle, and NSF China with 51575293, and U20A20334.

<sup>1</sup>School of Vehicle and Mobility, Tsinghua University, Beijing, 100084, China. <sup>2</sup>Institute for Interdisciplinary Information Sciences, Tsinghua University, Beijing, 100084, China. All correspondence should be sent to S. Eben Li. <lisb04@gmail.com>.

Data-driven PG methods only require data to learn a control policy. The PG theorem was first proposed by Sutton *et al.* (2000), who showed that the action-value (i.e., Q-value) function could be used to calculate the PG of stochastic policies [5]. The deterministic version of the PG (DPG) theorem was discovered by Silver *et al.* (2014). DPG also needs a Q-value to compute its gradient with respect to the action. In data-driven PG, imprecise value function may lead to poor PG, thereby negatively affecting policy performance. Therefore, in recent years, several tricks have been proposed to improve the estimation accuracy of value functions. Inspired by Deep Q Networks [2], Lillicrap *et al.* (2015) used a stochastic policy to explore in the environment to learn a more accurate Q-value function [6]. Besides, they introduced a target Q-value function to stabilize the learning process. Schulman *et al.* (2016) estimated the value function in the PG using an exponentially-weighted estimator that is analogous to TD( $\lambda$ ), substantially reducing the bias introduced by the learned value function [7]. Combining with techniques that guarantee monotonic improvement (such as TRPO and PPO [8], [9]), they yielded strong empirical results on highly challenging 3D locomotion tasks. Fujimoto *et al.* (2018) took the minimum value between a pair of Q-value functions to avoid overestimation [10]. Duan *et al.* proposed to learn a continuous return distribution to address value estimation errors, and achieved state-of-the-art performance on the suite of MuJoCo continuous control tasks [11]. However, learning an accurate value function in each update step is not practical, which leads to sample inefficiency. To tackle this, several studies learn a model from empirical data as a simulator to enhance sample efficiency. Their main focus is to deal with the bias in the model-generated data to achieve the same asymptotic performance as the above methods. Feinberg *et al.* (2018) presented model-based value expansion (MVE), which learns the value function using model predictions with fixed horizon [12]. Buckman *et al.* (2018) further proposed an extension to MVE called stochastic ensemble value expansion (STEVE), which interpolates between multiple different horizon lengths, favoring those with lower uncertainty estimates [13]. Similarly, Janner *et al.* (2019) used short model-generated rollouts branched from real data for both value and policy learning, matching the asymptotic performance of the best model-free methods [14]. These methods significantly improve the sample efficiency, but have no benefit on convergence speed cause there is no essential change in the way they update value functions and policies.

Model-driven PG methods require a differentiable model which can be either given as a prior or learned from empirical data. With the help of model, the analytical PG can be directly calculated by backpropagation of rewards along a trajectory. In

this way, the influence of the estimated value function on PG accuracy can be greatly reduced or even eliminated. A fairly precise PG can be obtained given a fair model, which is much easier than estimating from pure data. Therefore, leveraging model can speed up the convergence and further reduce the sample complexity. A pioneer work is PILCO proposed by Deisenroth and Rasmussen (2011), in which they learned a probabilistic model, and computed an analytical PG over a finite-horizon objective function to learn a deterministic policy. Results showed that PILCO can facilitate learning from scratch in only a few trials [15]. Heess *et al.* (2015) extended BPTT to infinite-horizon and stochastic policy using a learned value function and re-parameterization trick [16]. However, there are three main disadvantages of model-driven PG methods. The first one is the gradient exploding problem of the long chain of nonlinear computations shown in the back propagation process, which causes numerical instability in optimization. To address this problem, Parmas *et al.* (2019) developed a total propagation algorithm that introduces an additional PG estimator with the likelihood ratio trick and automatically gives greater weight to estimators with lower variance [17]. The second drawback is that the PG from BPTT is sensitive to model errors, especially for a long prediction-horizon [18]. This problem has also been shown in [16], in which a value function is integrated after certain forward steps driven by the model to increase robustness to model error and extend BPTT to infinite-horizon control. Their results also show that the asymptotic performance grows with the decrease of the prediction horizon, but the convergence speed becomes slower accordingly. Finally, the gradient computing time of BPTT grows linearly with the length of predictive horizon, which eliminates the benefits of fast convergence.

Since the data-driven PG and the model-driven PG have their respective merits and drawbacks, we propose a novel PG method driven by both empirical data and model to get benefits of both fast convergence and good asymptotic performance. Compared with some existing studies, the main contributions emphasize in three parts.

1) We propose a mixed policy gradient (MPG) method which interpolates between the data-driven PG and the model-driven PG to combine data and a prior model to benefit both convergence speed and asymptotic performance.

2) We unify the data-driven PG and the model-driven PG in a general form, and investigate the upper bound of their PG's errors. Relying on that, we propose a rule-based method to adaptively adjust the weights of the data-driven and model-driven PGs.

3) We propose an asynchronous learning architecture to address the poor computing efficiency suffered by BPTT, in which multiple learners are employed to compute the MPG in parallel to enhance update throughput.

## II. PRELIMINARY

We consider a Markov decision process (MDP) defined by the tuple  $(\mathcal{S}, \mathcal{A}, p, r, \gamma)$ .  $\mathcal{S}$  and  $\mathcal{A}$  are the state and action spaces, respectively, and  $\gamma \in (0, 1)$  is the discount factor. We denote the dynamics or transition distribution as  $p : \mathcal{S} \times \mathcal{A} \times \mathcal{S} \rightarrow [0, \infty)$ , and the reward function as  $r : \mathcal{S} \times \mathcal{A} \rightarrow \mathbb{R}$ . We use  $\pi : \mathcal{S} \rightarrow \mathcal{A}$  to denote a deterministic control policy and  $f : \mathcal{S} \times \mathcal{A} \times \mathcal{S} \rightarrow [0, \infty)$  to specify an employed model in the model-driven PG. For a deterministic MDP,  $p(\cdot|s, a)$  and  $f(\cdot|s, a)$  are Dirac measures. In this case, we denote  $p(s, a) = s'$  and  $f(s, a) = \hat{s}'$  as functions from  $\mathcal{S} \times \mathcal{A}$  to  $\mathcal{S}$ . We denote  $o$  as the observation with a random noise  $\epsilon$ , i.e.,  $o' = p(o, a) + \epsilon$ . We also use  $\rho^\pi(s)$  to denote the state distribution induced by policy  $\pi$  in dynamics  $p$ , which is defined in [19] as the discounted visiting frequency. We assume  $\rho^\pi$  has no gradient with respect to the policy. Unless otherwise stated,  $t$  is used as the start time,  $s_t = \hat{s}_t = o_t \sim \rho^\pi; a_t = \hat{a}_t; s_{t+1} \sim p(\cdot|s_t, a_t), s_{l+1} \sim p(\cdot|s_l, \pi(s_l)), l > t; \hat{s}_{t+1} \sim f(\cdot|\hat{s}_t, \hat{a}_t), \hat{s}_{l+1} \sim f(\cdot|\hat{s}_l, \pi(\hat{s}_l)), l > t; r_t := r(s_t, a_t), r_l := r(s_l, \pi(s_l)), l > t; \hat{r}_t := r(\hat{s}_t, \hat{a}_t), \hat{r}_l = r(\hat{s}_l, \pi(\hat{s}_l)), l > t$ . Let  $q^\pi$  be the Q-value function defined as:

$$q^\pi(s, a) = \mathbb{E}_{s_l, l > t} \left\{ \sum_{l=t}^{\infty} \gamma^{l-t} r_l \middle| s_t = s, a_t = a \right\}.$$

We approximate Q-value by  $Q(s, a; w) \approx q^\pi(s, a), \forall s \in \mathcal{S}, a \in \mathcal{A}$ , where  $w \in \mathbb{R}^{|w|}$ . We use  $Q_w$  or  $Q_w(s, a)$  for short. Besides, we approximate policy by  $\pi(s; \theta) \approx \pi(s), \forall s \in \mathcal{S}$ , where  $\theta \in \mathbb{R}^{|\theta|}$  and we use  $\pi_\theta$  or  $\pi_\theta(s)$  for short. Unless otherwise stated, we denote  $\hat{Q}_{w,t} := Q_w(\hat{s}_t, \hat{a}_t), \hat{Q}_{w,l} := Q_w(\hat{s}_l, \pi(\hat{s}_l)), l > t$ . The goal of RL is to find the optimal policy that maximizes the expected sum of discounted rewards. The objective function can be written as:

$$J(\theta) = \mathbb{E}_{s \sim d^0} \{q^{\pi_\theta}(s, \pi_\theta(s))\}. \quad (1)$$

where  $d^0$  is initial state distribution. From the theory of DPG, its gradient is

$$\nabla_\theta J(\theta) = \mathbb{E}_{s_t} \left\{ \nabla_{a_t} q^{\pi_\theta}(s_t, a_t) \middle|_{a_t=\pi_\theta(s_t)} \nabla_\theta \pi_\theta(s_t) \right\}. \quad (2)$$

For simplicity, we denote  $\mathbb{E}_s \{\nabla_a g \nabla_\theta \pi_\theta\} := \mathbb{E}_s \{\nabla_a g(s, a) |_{a=\pi_\theta(s)} \nabla_\theta \pi_\theta(s)\}$  through this paper, where  $g$  is any function of  $s$  and  $a$ . DPG (2) can be simplified as

$$\nabla_\theta J(\theta) = \mathbb{E}_{s_t} \{\nabla_{a_t} q^{\pi_\theta} \nabla_\theta \pi_\theta\}. \quad (3)$$

The data-driven PG is calculated by substituting  $q^{\pi_\theta}$  with its estimate  $Q_w$  in (2),

$$\nabla_\theta J^{\text{Data}}(\theta) = \mathbb{E}_{s_t} \{\nabla_{a_t} Q_w \nabla_\theta \pi_\theta\}. \quad (4)$$

The model-driven PG can be obtained by substituting  $q^{\pi_\theta}$  with  $n$ -step Bellman recursion in (1),

$$\nabla_\theta J_n^{\text{Model}}(\theta) = \nabla_\theta \mathbb{E}_{\hat{s}_t} \left\{ \nabla_\theta \mathbb{E}_{\substack{\hat{s}_{t+1}, \\ \vdots, \\ \hat{s}_{t+n}}} \left\{ \sum_{l=t}^{n-1+t} \gamma^{l-t} \hat{r}_l + \gamma^n \hat{Q}_{w,t+n} \right\} \right\}, \quad (5)$$

where  $\hat{s}_{t+i} \sim f(\cdot|\hat{s}_{t+i-1}, \pi_\theta(\hat{s}_{t+i-1})), i \geq 1; \hat{r}_{t+i} := r(\hat{s}_{t+i}, \pi_\theta(\hat{s}_{t+i})), i \geq 0$ .

### III. MIXED POLICY GRADIENT

#### A. Unified policy gradient

In this subsection, we propose a form of PG which unifies the concepts of both data-driven and model-driven PG to facilitate the following analysis. Different from existing model-driven PG methods, the unified PG directly replaces  $q^{\pi_\theta}(s, a)$  with  $n$ -step Bellman recursion in (2). The form of the unified PG is as follows,

$$\nabla_\theta J_n(\theta) = \mathbb{E}_{\hat{s}_t} \left\{ \nabla_{\hat{a}_t} \mathbb{E}_{\substack{\hat{s}_{t+1}, \dots, \\ \hat{s}_{t+n}}} \left\{ \sum_{l=t}^{n-1+t} \gamma^{l-t} \hat{r}_l + \gamma^n \hat{Q}_{w,t+n} \right\} \nabla_\theta \pi_\theta \right\} \quad (6)$$

Note that when  $n = 0$ , the unified PG is equivalent to the data-driven PG (4).

From (6), it is clear that the accuracy of the unified PG depends on model errors and Q-value estimate errors. In particular, as the predictive horizon  $n$  increases, the influence of estimate errors decays exponentially, while model errors accumulate continuously. Therefore, these two errors need to be balanced to get a relatively precise PG. Intuitively, during the early training stage, the estimated Q-value is far from its true value, so a larger  $n$  is preferred to reduce the reliance on the Q-value estimate. When the value function gradually converges, we need a smaller  $n$  to mitigate the influence of model errors. From this point of view, together with the Theorem 1, we can explain why the model-driven PG converges so fast.

**Lemma 1.** *If  $d^0 = d^\pi$  or  $\gamma \rightarrow 1$ ,*

$$\rho^\pi = d^\pi$$

where  $d^\pi$  is the stationary state distribution of the MDP under policy  $\pi$  and state transition dynamics  $p$ .

*Proof.* See Proposition 1 and Proposition 2 of [19].  $\square$

**Theorem 1.** *If  $f = p$  and  $\rho^\pi = d^\pi$  by Lemma 1, the model-driven PG (5) is a weighted average of the unified PG, i.e.,*

$$\nabla_\theta J_n^{\text{Model}}(\theta) = \sum_{k=0}^{n-1} \gamma^k \nabla_\theta J_{n-k}(\theta).$$

*Proof.* See Appendix A-B.  $\square$

The theorem shows that the weight of each unified PG  $\nabla_\theta J_{n-k}(\theta)$  in  $\nabla_\theta J_n^{\text{Model}}(\theta)$  increases exponentially with the prediction-horizon  $n - k$ . As a result, the model-based PG can greatly reduce the reliance on inaccurate Q-value estimate and converge fast. However, its asymptotic final performance is inevitably damaged by the model errors. The theorem enlightens us that if we can dynamically adjust the weights of unified PGs along the learning process, we may achieve fast learning with great asymptotic performance.

#### B. Upper bound analysis of the unified PG bias

In this subsection, we will derive the error of the unified PG and discuss its relation with model errors and Q-value estimate errors, so as to provide theoretical guidance for the development of the MPG algorithm. For simplicity, we will derive the upper bound of the error in the case of deterministic dynamics and models. Besides, throughout this paper, we will use  $\|\cdot\|$  to denote the Euclidean norm  $\|\cdot\|_2$ .

The bias of the unified PG is as follows,

$$\begin{aligned} & \|\nabla_\theta J_n(\theta) - \nabla_\theta J(\theta)\| \\ &= \left\| \mathbb{E}_{\hat{s}_t} \left\{ \left( \sum_{l=t}^{n-1+t} \gamma^{l-t} (\nabla_{\hat{a}_t} \hat{r}_l - \nabla_{\hat{a}_t} r_l) + \right. \right. \right. \\ & \quad \left. \left. \left. \gamma^n (\nabla_{\hat{a}_t} \hat{Q}_{w,t+n} - \nabla_{\hat{a}_t} q_{t+n}^{\pi_\theta}) \right) \nabla_\theta \pi_\theta \right\} \right\| \end{aligned} \quad (7)$$

where we expand  $q^{\pi_\theta}(s, a)$  in (2) by  $n$ -step Bellman recursion, and denote  $q_t^{\pi_\theta} := q^{\pi_\theta}(\hat{s}_t, \hat{a}_t)$ ,  $q_{t+n}^{\pi_\theta} := q^{\pi_\theta}(s_{t+n}, \pi_\theta(s_{t+n}))$ ,  $n > 0$ . All gradient terms in (7) can be easily calculated according to the chain rule. See Appendix A-A for details.

To further derive the error of the unified PG, we first state the following conditions about model errors and data errors. The other conditions are shown in Appendix A-C.

**Condition 1.**  *$p(s, a) = f(s, a) + \delta(s, a)$ , where  $\delta(s, a)$  is an error function of model, and model state error grows linearly with prediction horizon, i.e.,  $\sup_{\hat{s}_t \in \mathcal{S}, \hat{a}_t \in \mathcal{A}} \|s_{t+i} - \hat{s}_{t+i}\| \leq c_m i$ , where  $c_m$  is a constant.*

The errors of  $Q_w(s, a)$  consist of two parts. One is the error caused by observation noise  $\epsilon$ , and the other is the function approximation error. For the former, the Q-value corresponding to the experience with noise is exactly that of an MDP with the dynamics  $o' = p(o, a) + \epsilon$ . We denote the *noisy* Q-value as  $q^{\pi_\theta, o}$  and derive the upper bound of the difference between its gradient and that of the true Q-value, as shown in Lemma 2. For the latter, we have the Condition 2, in which the bounds  $B_{qs}$  and  $B_{qa}$  are served as the indicator of the function approximate error. And they are expected to be a small value when we have well estimated Q-values, and vice versa.

**Condition 2.** *The difference of the gradient of the estimated Q-value and the noisy Q-value is bounded.*

$$\begin{aligned} \sup_{s \in \mathcal{S}} \|\nabla_s Q_w(s, \pi_\theta(s)) - \nabla_s q^{\pi_\theta, o}(s, \pi_\theta(s))\| &= B_{qs} \\ \sup_{s \in \mathcal{S}, a \in \mathcal{A}} \|\nabla_a Q_w(s, a) - \nabla_a q^{\pi_\theta, o}(s, a)\| &= B_{qa} \end{aligned}$$

**Lemma 2.** *Given regular conditions of continuity and boundedness shown in Appendix A-C, we have*

$$\begin{aligned} \sup_{s \in \mathcal{S}} \|\nabla_s q^{\pi_\theta}(s, \pi_\theta(s)) - \nabla_s q^{\pi_\theta, o}(s, \pi_\theta(s))\| &\leq \text{const} \cdot \mathbb{E}_\epsilon \{\|\epsilon\|\} \\ \sup_{s \in \mathcal{S}, a \in \mathcal{A}} \|\nabla_a q^{\pi_\theta}(s, a) - \nabla_a q^{\pi_\theta, o}(s, a)\| &\leq \text{const} \cdot \mathbb{E}_\epsilon \{\|\epsilon\|\} \end{aligned}$$

*Proof.* See Appendix A-D.  $\square$

We can now study the upper bound of  $\|\nabla_{\hat{a}_t} \hat{r}_{t+k} - \nabla_{\hat{a}_t} r_{t+k}\|$ ,  $k \geq 0$  and  $\|\nabla_{\hat{a}_t} \hat{Q}_{w,t+k} - \nabla_{\hat{a}_t} q_{t+k}^{\pi_\theta}\|$ ,  $k \geq 0$ , and derive the following Lemma.

**Lemma 3.** *Given Condition 1, Condition 2 and regular conditions of continuity and boundedness shown in Appendix A-C, we have*

$$\begin{aligned} \sup_{\hat{s}_t \in \mathcal{S}, \hat{a}_t \in \mathcal{A}} \|\nabla_{\hat{a}_t} \hat{r}_{t+k} - \nabla_{\hat{a}_t} r_{t+k}\| &\leq U_r(k), k \geq 0 \\ \sup_{\hat{s}_t \in \mathcal{S}, \hat{a}_t \in \mathcal{A}} \|\nabla_{\hat{a}_t} \hat{Q}_{w,t+k} - \nabla_{\hat{a}_t} q_{t+k}^{\pi_\theta}\| &\leq U_q(k), k \geq 0, \end{aligned}$$

where,

$$\begin{aligned} U_r(k) &= \begin{cases} o((c_m k)^k), & k \geq 1 \\ 0, & k = 0 \end{cases} \\ U_q(k) &= \begin{cases} o((c_m k)^k) + \text{const} \cdot (B_{qs} + \mathbb{E}_\epsilon \{\|\epsilon\|\}), & k \geq 1 \\ B_{qa} + \text{const} \cdot \mathbb{E}_\epsilon \{\|\epsilon\|\}, & k = 0 \end{cases} \end{aligned}$$

*Proof.* See Appendix A-E.  $\square$

Finally, we give the upper bound of the bias of the unified PG by the following theorem.

**Theorem 2.** *Given Condition 1, Condition 2, and regular conditions of continuity and boundedness shown in Appendix A-C, we have*

$$\begin{aligned} \|\nabla_\theta J_n(\theta) - \nabla_\theta J(\theta)\| &\leq \\ \begin{cases} o(n(\gamma c_m n)^n) + \gamma^n \text{const} \cdot (B_{qs} + \mathbb{E}_\epsilon \{\|\epsilon\|\}), & n \geq 1 \\ \text{const} \cdot (B_{qa} + \mathbb{E}_\epsilon \{\|\epsilon\|\}), & n = 0 \end{cases} \end{aligned}$$

*Proof.* See Appendix A-F.  $\square$

From the Theorem 2, it can be seen that the upper bound of the unified gradient error is determined by model errors and Q-value errors (including observation noise and function approximate error). Specifically, when the prediction horizon  $n = 0$ , the unified PG degenerates into the data-driven PG (4). The PG error is only influenced by Q-value errors, i.e.,  $\text{const} \cdot (B_{qa} + \mathbb{E}_\epsilon \{\|\epsilon\|\})$ . When the prediction horizon  $n \geq 1$ , the unified PG error is determined by both model errors  $o(n(\gamma c_m n)^n)$  and Q-value estimate errors  $\gamma^n \text{const} \cdot (B_{qs} + \mathbb{E}_\epsilon \{\|\epsilon\|\})$ . Besides, with the increase of the prediction horizon, the PG error caused by model errors grows exponentially. On the contrary, that caused by Q-value estimate errors is controlled by the discount factor and decreases exponentially. When the prediction horizon increases to infinity, the PG error is only related to model errors. However, in that case, the model errors can make the unified PG arbitrarily bad.

We can be enlightened by Theorem 2 in the following ways. At the beginning of training, when the Q-value errors have much more influence on the PG error compared with model errors, we can ignore the model error term  $o(n(\gamma c_m n)^n)$  and discover that the PG error decreases exponentially with  $n$ . At the late phase of training, when the Q-value is well estimated, the Q-value errors become negligible, then the PG error increases exponentially with  $n$  because of the model error term. These findings from the Theorem 2 can be applied to the design of the weights of the MPG.

### C. Mixed policy gradient

For simplicity, MPG is designed as a weighted average of two special unified PGs, i.e.  $\nabla_\theta J_0(\theta)$  and  $\nabla_\theta J_\infty(\theta)$ . The former is purely driven by data and the latter is purely

driven by model. However, constructing an infinite Bellman recursion is impractical and  $\nabla_\theta J_\infty(\theta)$  has no upper bound from Theorem 2, so we replace  $\nabla_\theta J_\infty(\theta)$  with  $\nabla_\theta J_H(\theta)$ , where  $H$  is a large number. The form of the MPG is as follows,

$$\nabla_\theta J^{\text{Mixed}}(\theta) = w_0 \nabla_\theta J_0(\theta) + w_H \nabla_\theta J_H(\theta),$$

where  $w_0$  and  $w_H$  are the weights to be determined. The MPG can be extended in a more general form by weighted average of multiple unified PGs with different horizons. See Appendix C-A for detailed descriptions.

To calculate the MPG, we first construct its corresponding policy loss function, i.e.,

$$\begin{aligned} J^{\text{Mixed}}(\theta) &= w_0 J_0(\theta) + w_H J_H(\theta) \\ &= w_0 \mathbb{E}_{\hat{s}_t \sim \rho^{\pi_{\theta_{\text{old}}}} \{X_0(\hat{s}_t; \theta)\}} + w_H \mathbb{E}_{\hat{s}_t \sim \rho^{\pi_{\theta_{\text{old}}}} \{X_H(\hat{s}_t; \theta)\}} \\ &= \mathbb{E}_{\hat{s}_t \sim \rho^{\pi_{\theta_{\text{old}}}}} \{w_0 X_0(\hat{s}_t; \theta) + w_H X_H(\hat{s}_t; \theta)\}, \end{aligned} \quad (8)$$

where  $J_0$  and  $J_H$  are losses derived inversely from the unified PG (6). Specifically,  $X_i(\hat{s}_t; \theta) := \mathbb{E}_{\hat{s}_{t+1}, \dots, \hat{s}_{t+i}} \left\{ \sum_{l=t}^{i-1+t} \gamma^{l-t} \hat{r}_l + \gamma^i \hat{Q}_{w,t+i} \right\}$ ,  $\hat{s}_{t+1} \sim f(\cdot | \hat{s}_t, \pi_\theta(\hat{s}_t))$ ,  $\hat{s}_{t+i} \sim f(\cdot | \hat{s}_{t+i-1}, \pi_{\theta_{\text{old}}}(\hat{s}_{t+i-1}))$ ,  $i > 1$ ;  $\hat{r}_t := r(\hat{s}_t, \pi_\theta(\hat{s}_t))$ ,  $\hat{r}_{t+i} := r(\hat{s}_{t+i}, \pi_{\theta_{\text{old}}}(\hat{s}_{t+i}))$ ,  $i > 0$ ;  $\hat{Q}_{w,t} := Q_w(\hat{s}_t, \pi_\theta(\hat{s}_t))$ ,  $\hat{Q}_{w,t+i} := Q_w(\hat{s}_{t+i}, \pi_{\theta_{\text{old}}}(\hat{s}_{t+i}))$ ,  $i > 0$ ,  $\theta_{\text{old}} = \theta$ .

According to [20], the state distribution  $\pi_{\theta_{\text{old}}}$  in (8) can be safely replaced with that of an arbitrary policy  $b$ . This property naturally transforms the MPG into a more general off-policy version, shown as,

$$J^{\text{Mixed}}(\theta) = \mathbb{E}_{\hat{s}_t \sim \rho^b} \{w_0 X_0(\hat{s}_t; \theta) + w_H X_H(\hat{s}_t; \theta)\}. \quad (9)$$

This formula reveals the process to compute the MPG: we first sample a batch of  $\hat{s}_t$  from the state distribution  $\rho^b$ . Then, we compute all model returns  $X_0(\hat{s}_t; \theta)$  and  $X_H(\hat{s}_t; \theta)$  for each  $\hat{s}_t$  and decide the weights  $w_0$  and  $w_H$  to compute the loss function. Finally, we take its gradient to get the MPG. The MPG algorithm is shown in Algorithm 1.

The MPG algorithm can be interpreted as a way to balance the variance of the data-driven loss and the bias of model-driven loss, as shown in Figure 1. The data-driven PG methods construct  $J_0(\theta)$  relying on the estimated Q-value. Because the Q-value changes with policies during the learning process,  $J_0(\theta)$  is served as the local approximation of the true loss (1), which is inaccurate with a large variance in the early training phase, resulting in a bad policy update. But with the Q-value converges, the local approximation is of high quality, then the optimal solution can be found. For model-driven PG, the loss function  $J_\infty(\theta)$  is only determined by the model which is invariant during training, but is with bias due to the mismatch between the model and the true dynamics of the environment, which leads to a sub-optimal solution. The MPG algorithm mixes the two loss functions dynamically by weighted average to construct a better approximation of the true loss.

## IV. PRACTICAL ALGORITHM

### A. Weighting method

According to Theorem 2, we employ a simple rule-based method to determine the weights of  $J_0$  and  $J_H$ . Specifically,

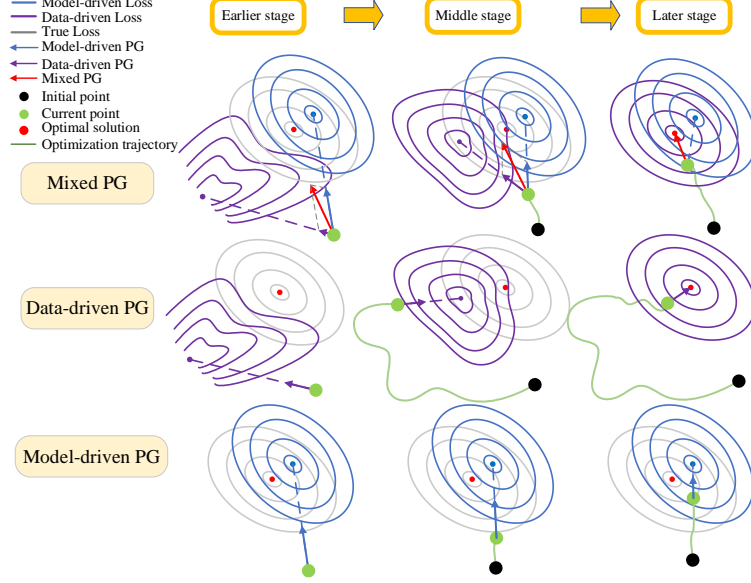


Fig. 1: Interpretation of MPG. The loss of data-driven PG converges to the true loss along training process but has large variance in the earlier state. The loss of model-driven PG has low variance but is biased. Mixed PG dynamically adjusts the weights of the data loss and the model loss to construct a better approximation of the true loss function.

we have the following prior assumptions: 1. The Q-value errors are dominant compared with the model error at the beginning of training; 2. The Q-value errors become negligible when the Q-value is well estimated in the late training phase, while the model errors dominate the PG error. Then from Theorem 2, the unified PG error decreases exponentially with the prediction horizon in the earlier training phase, but increases exponentially in the late training phase. Guided by the findings, we first design a rule-based error for a given prediction horizon  $i$ , which is a piecewise function that consists of two exponential functions. The base number  $\lambda$  is an independent variable and is designed to grow continuously with the learning process. When  $\lambda \leq 1$ , the error will exponentially decrease with the prediction horizon, and vice versa. Next, the inverses of the calculated rule-based errors are passed to a Softmax operator to obtain the weights. The calculation details are shown below,

$$w_i = \text{Softmax}(1/\text{Rule-Error}_i), i = 0, H$$

$$\text{Rule-Error}_i = \begin{cases} \lambda^i, & \lambda \leq 1 \\ (2 - \lambda)^{H-i}, & \lambda > 1 \end{cases}, \quad (10)$$

where  $\lambda$  is a variable that linearly increases from  $1 - \eta$  to  $1 + \eta$  within iteration  $T$  and remain  $1 + \eta$  thereafter,  $\eta \in (0, 1)$  and  $T$  are served as hyperparameters.

### B. Value learning

To learn the action-value function, we minimize the mean squared error between the approximate value function and target values, i.e.,

$$\min_w J_Q(w) = \mathbb{E}_{s,a} \left\{ \frac{1}{2} (R^{\text{Target}}(s, a) - Q_w(s, a))^2 \right\},$$

where  $s, a$  obey arbitrary joint distributions. Depending on how to calculate  $R^{\text{Target}}$ , we develop two variants of the MPG,

---

### Algorithm 1 Mixed Policy Gradient

---

**Initialize:** critic network  $Q_w$  and actor network  $\pi_\theta$  with random parameters  $w, \theta$ , target parameters  $w' \leftarrow w, \theta' \leftarrow \theta$ , batch size  $N$ , initial buffer  $\mathcal{B}$  with  $N$  samples, update interval  $m$ , exploration noise  $\epsilon$ , target smoothing coefficient  $\tau$ , learning rates  $\beta_w, \beta_\theta$   
**for** each iteration  $k$  **do**  
    Collect a batch of transitions using  $\pi_\theta$  with noise  $\epsilon$ , store in  $\mathcal{B}$   
    Sample  $N$  transitions  $\{s_i, a_i, r_i, s_{i+1}\}_{i=0:N-1}$  from  $\mathcal{B}$   
    Update value  $w \leftarrow w - \beta_w \nabla_w J_Q(w)$  using (12)  
    **if**  $k \bmod m$  **then**  
        Compute  $w_0, w_H$  by (10)  
        Compute  $J^{\text{Mixed}}(\theta)$  using (9)  
        Update policy  $\theta \leftarrow \theta + \beta_\theta \nabla_\theta J^{\text{Mixed}}(\theta)$   
        Update target networks:  
             $w' \leftarrow \tau w + (1 - \tau)w'$   
             $\theta' \leftarrow \tau \theta + (1 - \tau)\theta'$   
    **end if**  
**end for**

---

i.e., MPG-v1 and MPG-v2, where the former uses  $n$ -step TD method, and the latter employs clipped double Q method developed by Fujimoto *et al.* [10].

$$R^{\text{Target}}(s_t, a_t) = \begin{cases} \sum_{l=t}^{t+n-1} \gamma^{l-t} r_l + \gamma^n Q_{w'}(s_{t+n}, \pi_{\theta'}(s_{t+n})), & \text{MPG-v1} \\ r_t + \gamma \min_{i=1,2} Q_{w'_i}(s_{t+1}, \pi_{\theta'}(s_{t+1})), & \text{MPG-v2} \end{cases} \quad (11)$$

For MPG-v1, the calculation of the  $n$ -step TD requires running the current policy in the environment starting from each state in the batch. The procedure can be one of the bottlenecks

of update throughput if the environment has low sampling efficiency. To solve the problem, we propose a batch reuse technique to improve sample utilization, in which a batch of data and its correlated target are used several times to compute gradients. Besides, the problem can also be alleviated by updating asynchronously. The value parameters can be optimized with gradients

$$\nabla_w J_Q(w) = -\mathbb{E}_{s,a} \{(R^{\text{Target}}(s, a) - Q_w(s, a)) \nabla_w Q_w(s, a)\}. \quad (12)$$

### C. Asynchronous learning architecture

The wall-clock time to converge equals to the product of the required iteration number and the time consumption of per iteration. The former is determined completely by the algorithms, while the latter (inversely proportional to the update throughput) consists of two parts in a serial learning architecture. One is the time for computing the PG, and the other is the time for applying it. Although MPG has great convergence speed w.r.t. iteration number, the computing time of MPG is roughly proportional to the predictive horizon  $H$ , resulting in lower computation efficiency than data-driven PG methods. We propose an asynchronous learning architecture to reduce the time consumption per iteration by eliminating the time for waiting a PG to be computed, so as to match the update throughput of data-driven PG methods. In the architecture, Buffers, Actors and Learners are all distributed across multiple processes to improve the efficiency of replay, sampling, and PG computation, as shown in Fig. 2.

The Optimizer is the core module, which is in charge of creating and coordinating other processes. The Optimizer owns the latest parameters, a gradient queue, an experience queue and an update thread, which keeps fetching gradients from the gradient queue and updating the parameters. The Optimizer also creates an Evaluator and several Actors, Buffers and Learners in separate processes. Each Actor owns local parameters and the environment to generate experience. They asynchronously synchronize the parameters from the Optimizer, and send the generated experience to a random Buffer. The Buffers receive the experience collected by the Actors and keep sampling batch data to the experience queue. Each Learner owns local parameters and a loss function defined by an RL algorithm to compute the gradients of the parameters. They asynchronously synchronize the parameters from the Optimizer, sample experience from the experience queue, and send gradients to the gradient queue for updating. The Evaluator contains local parameters, an environment and metrics. It asynchronously synchronizes the parameters from the Optimizer, runs the trained policy in the environment to compute the metrics for evaluating the policies along the training process.

One drawback of the asynchronous learning architecture is the staleness of the gradient, which is defined as the iteration number that has occurred between its parameter synchronization and update operations. We control the staleness by fixing the update queue capacity to a low value, as does in [21].

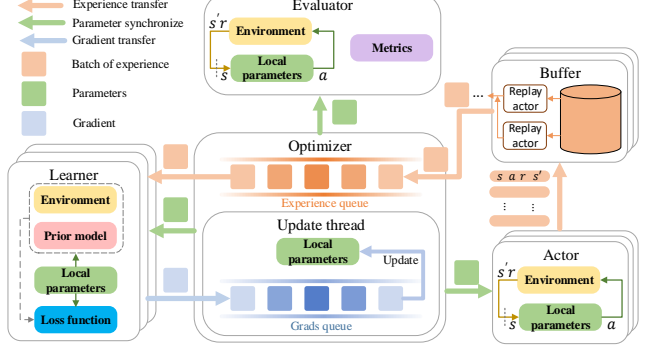


Fig. 2: Asynchronous learning architecture. Buffers, Actors and Learners are all distributed across multiple processes to improve the efficiency of replay, sampling, and PG computation. The time consumption per iteration of MPG can be significantly reduced by employing more Learners.

## V. EXPERIMENT

### A. Simulators and prior models

We conduct experiments on both path tracking task and inverted pendulum task, as shown in Fig. 6. In the path tracking task, the autonomous vehicle is required to track the given path and velocity to minimize the tracking errors. We develop a highly parallelized simulator for this task, which allows hundreds of agents to run simultaneously. The inverted pendulum task is adapted from the Gym package to make its reward an explicit function of states and actions, which is also used by its prior model. The task uses MuJoCo as its simulator. The prior models need to be deterministic and differentiable w.r.t the state and action to construct the MPG through BPTT. To test the effectiveness of our methods, we take several measures to enlarge the mismatch between the model and the true dynamics in the simulator, such as adding biased noise in the transition model, using different discrete time step, etc. Detailed task design and prior model are shown in Appendix B.

### B. Experiments and results

We compare our algorithm against  $n$ -step deterministic policy gradient ( $n$ -step DPG), a data-driven algorithm which is modified on deep deterministic policy gradient (DDPG) by replacing the value target with  $n$ -step Bellman recursion;  $n$ -step adaptive dynamic programming ( $n$ -step ADP), a model-driven algorithm that extends one-step adaptive dynamic programming (ADP) to  $n$ -step in both value and policy learning. Additionally, we compare our method to twin delayed deep deterministic policy gradient algorithm (TD3), an extension to DDPG which first applied the double Q-learning trick to continuous control along with other improvements; soft actor-critic (SAC), an algorithm which is regarded as the state-of-the-art off-policy deep RL method. The source code of our MPG implementation<sup>1</sup> is available online.

<sup>1</sup><https://github.com/idthanm/mpg/>

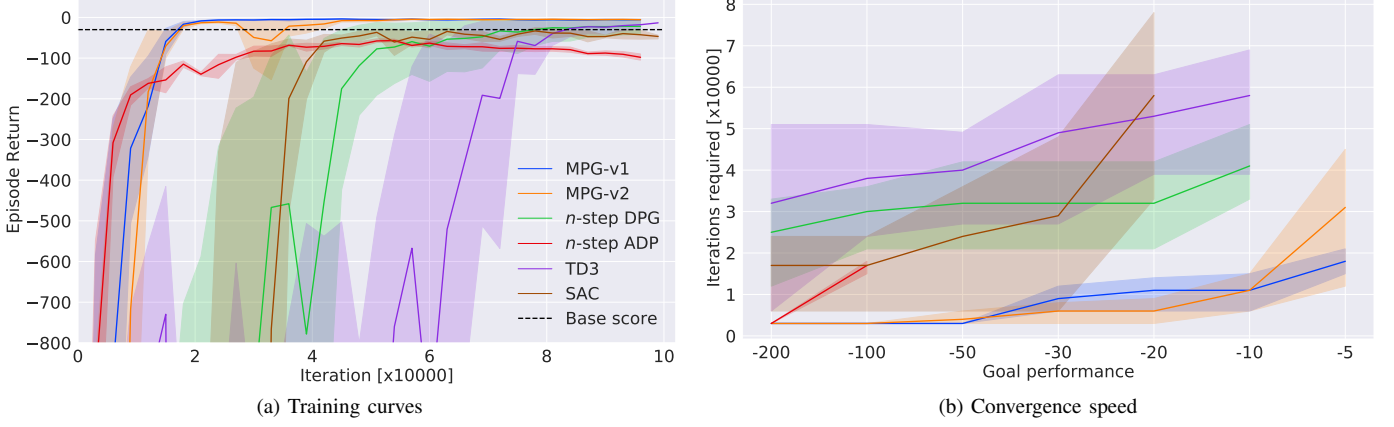


Fig. 3: Algorithm comparison in terms of asymptotic performance and convergence speed on the path tracking task. (a) Training curves. The dashed line shows the minimum requirement for the task to work, which is -30 in the task (see Appendix B for its calculation). (b) Convergence speed of different algorithms, which is measured by the average number of iterations needed to reach a certain goal performance. The missing part of the curves on some goal performances means that the algorithms never reached these goals. The solid lines correspond to the mean and the shaded regions correspond to 95% confidence interval over 5 runs.

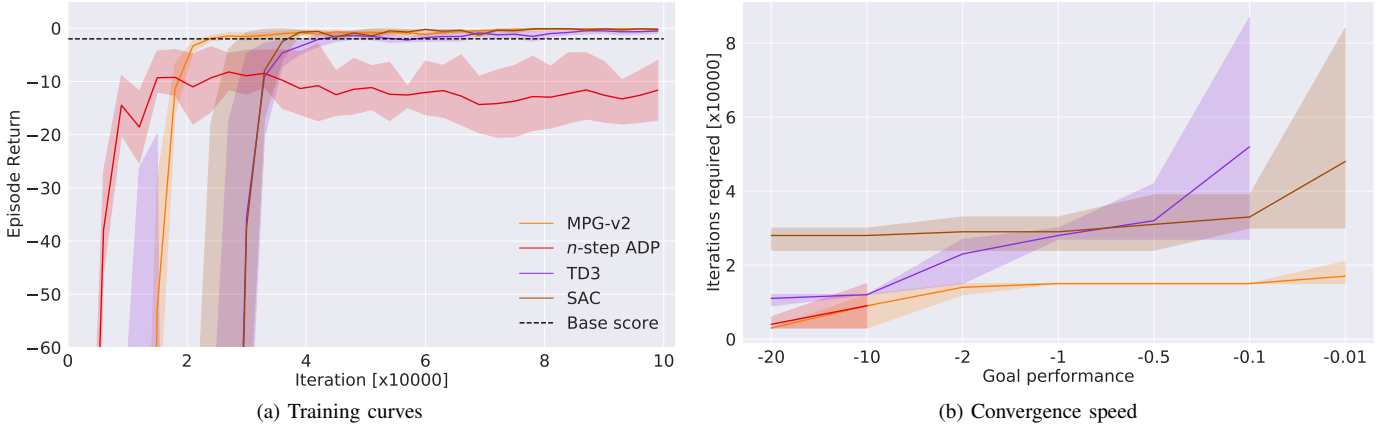


Fig. 4: Algorithm comparison in terms of asymptotic performance and convergence speed on the inverted pendulum task. (a) Training curves. The dashed line shows the minimum requirement for the task to work, which is -2 in the task (see Appendix B for its calculation). (b) Convergence speed of different algorithms. The MPG-v1 and n-step DPG fail on this task because of the n-step TD value learning, so they are not plotted. The solid lines correspond to the mean and the shaded regions correspond to 95% confidence interval over 5 runs.

1) *Performance*: All the algorithms mentioned above are implemented in the asynchronous learning architecture proposed in section IV-C, including 2 Actors, 2 Buffers, and 12 Learners. For action-value functions and policies, we use a fully connected neural network (NN) with 2 hidden layers, consisting of 256 units per layer, with Exponential Linear Units (ELU) each layer [22]. For stochastic policies, we use a Gaussian distribution with mean and covariance given by a NN, where the covariance matrix is diagonal. The Adam method [23] with a polynomial decay learning rate is used to update all the parameters. Specific hyperparameter settings are listed in Appendix C-C.

We train 5 different runs of each algorithm with different random seeds, with evaluations every 3000 iterations. Each

evaluation calculates the average return over 5 episodes without exploration noise, where each episode has a fixed 200 time steps (100 for inverted pendulum task). We illustrate the algorithm performance in terms of its asymptotic performance and convergence speed. The former is measured by the episode return during training, and the latter is measured by the number of iterations needed to reach a certain goal performance. The curves are shown in Fig. 3 and Fig. 4, and results in Table I. The MPG (v1 and v2), n-step DPG, and n-step ADP use mixed PG, data-driven PG and model-driven PG for policy learning, respectively (See Appendix C-B).

Results show that, on the path tracking task, MPG-v1 and MPG-v2 outperform all the baseline methods with a large margin, both in terms of the asymptotic performance and

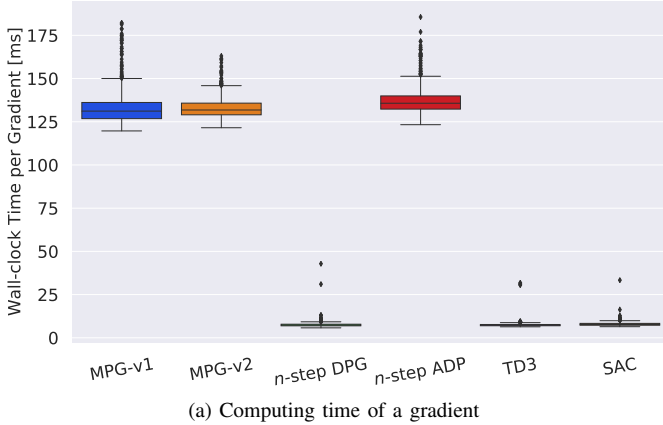
TABLE I: ASYMPTOTIC PERFORMANCE AND CONVERGENCE SPEED OVER 5 RUNS OF 100 THOUSAND ITERATIONS. THE BEST VALUE FOR EACH TASK IS BOLDED.  $\pm$  CORRESPONDS TO 95% CONFIDENCE INTERVAL OVER RUNS. THE CONVERGENCE SPEED IS MEASURED BY THE AVERAGE ITERATIONS NEEDED TO REACH A CERTAIN PERFORMANCE.

Task	Algorithm	Performance	Convergence speed (-100, -20) <sup>*</sup>	Convergence speed (-30, -2)	Convergence speed (-10, -0.1)	Convergence speed (-5, -0.01)
Path tracking	MPG-v1 (ours)	<b>-3.73 <math>\pm</math> 1.16</b>	<b>3000 <math>\pm</math> 0</b>	9000 $\pm$ 4898	<b>11000 <math>\pm</math> 7483</b>	<b>18000 <math>\pm</math> 4898</b>
	MPG-v2 (ours)	-4.60 $\pm$ 1.40	3000 $\pm$ 0	<b>6000 <math>\pm</math> 4898</b>	11000 $\pm$ 7483	31000 $\pm$ 27856
	<i>n</i> -step DPG	-21.89 $\pm$ 47.87	30000 $\pm$ 12961	32000 $\pm$ 17204	41000 $\pm$ 14966	-
	<i>n</i> -step ADP	-56.83 $\pm$ 7.44	17000 $\pm$ 2828	-	-	-
	TD3	-13.30 $\pm$ 26.50	38000 $\pm$ 22090	49000 $\pm$ 31496	58000 $\pm$ 26981	-
	SAC	-33.18 $\pm$ 19.97	17000 $\pm$ 15748	29000 $\pm$ 34756	-	-
Inverted Pendulum <sup>†</sup>	MPG-v2 (ours)	<b>-0.08 <math>\pm</math> 0.16</b>	<b>3000 <math>\pm</math> 0</b>	<b>14000 <math>\pm</math> 2828</b>	<b>15000 <math>\pm</math> 0</b>	<b>17000 <math>\pm</math> 5656</b>
	<i>n</i> -step ADP	-8.22 $\pm$ 7.64	4000 $\pm$ 2828	-	-	-
	TD3	-0.48 $\pm$ 1.35	11000 $\pm$ 22090	23000 $\pm$ 11313	52000 $\pm$ 50990	-
	SAC	-0.09 $\pm$ 0.12	28000 $\pm$ 5656	29000 $\pm$ 7483	33000 $\pm$ 8485	48000 $\pm$ 50911

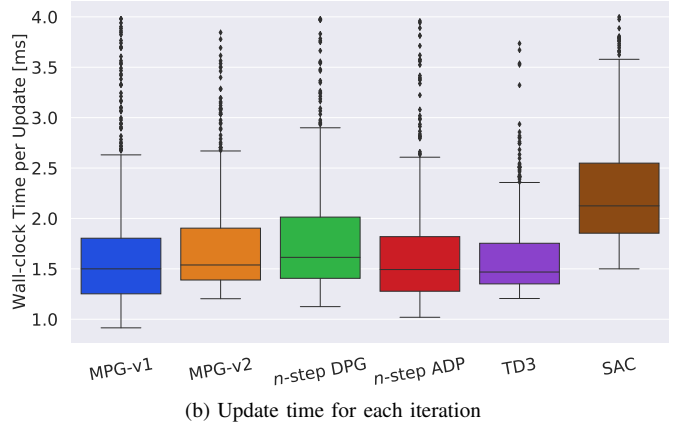
<sup>†</sup> MPG-v1 and *n*-step DPG fail on this task.

<sup>\*</sup> The goal performance for path tracking and inverted pendulum tasks, respectively.

- The algorithm never reached the goal performance.



(a) Computing time of a gradient



(b) Update time for each iteration

Fig. 5: Algorithm comparison in terms of time efficiency on the path tracking task. (a) Computing time of a policy gradient. (b) Update time for each iteration. Each boxplot is drawn based on all evaluations over 5 runs. All evaluations were performed on a single computer with a 2.4 GHz 50 core Inter Xeon CPU.

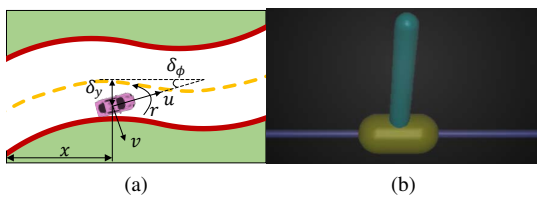


Fig. 6: Tasks. (a) Path tracking task:  $(s, a) \in \mathbb{R}^6 \times \mathbb{R}^2$ . (b) Inverted pendulum task:  $(s, a) \in \mathbb{R}^4 \times \mathbb{R}^1$ .

convergence speed. For example, on the path tracking task, *n*-step DPG uses data-driven PG and the same policy evaluation method as MPG. However, it is much slower than MPG and converges to a worse policy with larger variance. *n*-step ADP uses model-driven PG, as a result, it converges fast but leads to the worst asymptotic performance because of model errors. MPG also learns considerably faster than TD3 and SAC with better final performance and smaller variance. This is because that these data-driven baselines compute PG totally depending

on the action-value function, which is hard to learn well in the early phase of the training process. On the inverted pendulum task, MPG-v2 yields the best result, but MPG-v1 and *n*-step DPG algorithm fail to learn a feasible policy. It is because both of them use *n*-step TD learning, which suffers from large variance on that task, i.e., slightly change in the policy may lead to different orders of magnitude of returns. The quantitative results attained by MPG indicate that the mixture of data-driven PG and model-driven PG helps to obtain both their benefits.

2) *Time efficiency*: Figure 5 compares the time efficiency of different algorithms on the path tracking task. Results show that the average wall-clock time to compute a gradient of MPG, together with *n*-step ADP, is much higher than *n*-step DPG, TD3 and SAC. This is because the time for BPTT grows linearly with the length of time chain, which is set to be 25 in our experiment. If we employ a synchronous learning architecture, the fast convergence advantage of MPG would be offset by the slow gradient computing time. Therefore, we develop an asynchronous learning architecture to address this

problem, in which we use several learners to accelerate the gradient generation. As a result, we reduce the update time of MPG as well as  $n$ -step ADP to the level of data-driven RL methods, in which there is no need to wait for a gradient to be computed and all the time is used to update the value and policy networks.

## VI. CONCLUSION

In this paper, we presented mixed policy gradient (MPG), an off-policy deep reinforcement learning algorithm which uses both empirical data and a prior model to construct a mixture of data-driven PG and model-driven PG so as to get benefits in terms of both asymptotic performance and convergence speed. The data-driven PG uses the learned action-value function in the DPG to compute its derivative with respect to the action, whereas the model-driven PG uses the model rollout to compute  $n$ -step Bellman recursion to approximate the action-value function in the DPG and computes the derivative by BPTT. Our theoretical results show that these two types of PG can be unified and their deviation from the true PG can be bounded by the model error and the estimates error of the action-value function. Relying on this, we propose a rule-based weighting method to obtain the MPG, which is used to balance the bias of the model and the action-value function while avoiding the impacts caused by BPTT of long-chain nonlinear computation. Besides, an asynchronous learning architecture is proposed to reduce the wall-clock time needed for each update to the level of data-driven RL. We evaluate our method on the path tracking task and inverted pendulum task. Results show that the proposed MPG algorithm outperforms all baseline algorithms with a large margin in terms of both asymptotic performance and convergence speed.

## REFERENCES

- [1] S. E. Li, *Reinforcement learning and control. Lecture notes of Tsinghua University*, 2019.
- [2] V. Mnih, K. Kavukcuoglu, D. Silver, A. A. Rusu, J. Veness, M. G. Bellemare, A. Graves, M. Riedmiller, A. K. Fidjeland, G. Ostrovski *et al.*, “Human-level control through deep reinforcement learning,” *Nature*, vol. 518, no. 7540, p. 529, 2015.
- [3] Y. Guan, Y. Ren, S. E. Li, Q. Sun, L. Luo, and K. Li, “Centralized cooperation for connected and automated vehicles at intersections by proximal policy optimization,” *IEEE Transactions on Vehicular Technology*, vol. 69, no. 11, pp. 12 597–12 608, 2020.
- [4] O. Vinyals, I. Babuschkin, W. M. Czarnecki, M. Mathieu, A. Dudzik, J. Chung, D. H. Choi, R. Powell, T. Ewalds, P. Georgiev *et al.*, “Grandmaster level in starcraft ii using multi-agent reinforcement learning,” *Nature*, pp. 1–5, 2019.
- [5] R. S. Sutton, D. A. McAllester, S. P. Singh, and Y. Mansour, “Policy gradient methods for reinforcement learning with function approximation,” in *Advances in neural information processing systems*, 2000, pp. 1057–1063.
- [6] T. P. Lillicrap, J. J. Hunt, A. Pritzel, N. Heess, T. Erez, Y. Tassa, D. Silver, and D. Wierstra, “Continuous control with deep reinforcement learning,” *arXiv preprint arXiv:1509.02971*, 2015.
- [7] J. Schulman, P. Moritz, S. Levine, M. Jordan, and P. Abbeel, “High-dimensional continuous control using generalized advantage estimation,” *arXiv preprint arXiv:1506.02438*, 2015.
- [8] J. Schulman, S. Levine, P. Abbeel, M. Jordan, and P. Moritz, “Trust region policy optimization,” in *International Conference on Machine Learning*, 2015, pp. 1889–1897.
- [9] J. Schulman, F. Wolski, P. Dhariwal, A. Radford, and O. Klimov, “Proximal policy optimization algorithms,” *arXiv preprint arXiv:1707.06347*, 2017.
- [10] S. Fujimoto, H. van Hoof, and D. Meger, “Addressing function approximation error in actor-critic methods,” *arXiv preprint arXiv:1802.09477*, 2018.
- [11] J. Duan, Y. Guan, S. E. Li, Y. Ren, and B. Cheng, “Distributional soft actor-critic: Off-policy reinforcement learning for addressing value estimation errors,” *arXiv preprint arXiv:2001.02811*, 2020.
- [12] V. Feinberg, A. Wan, I. Stoica, M. I. Jordan, J. E. Gonzalez, and S. Levine, “Model-based value estimation for efficient model-free reinforcement learning,” *arXiv preprint arXiv:1803.00101*, 2018.
- [13] J. Buckman, D. Hafner, G. Tucker, E. Brevdo, and H. Lee, “Sample-efficient reinforcement learning with stochastic ensemble value expansion,” in *Advances in Neural Information Processing Systems*, 2018, pp. 8224–8234.
- [14] M. Janner, J. Fu, M. Zhang, and S. Levine, “When to trust your model: Model-based policy optimization,” in *Advances in Neural Information Processing Systems*, 2019, pp. 12 498–12 509.
- [15] M. Deisenroth and C. E. Rasmussen, “Pilco: A model-based and data-efficient approach to policy search,” in *Proceedings of the 28th International Conference on machine learning (ICML-11)*, 2011, pp. 465–472.
- [16] N. Heess, G. Wayne, D. Silver, T. Lillicrap, T. Erez, and Y. Tassa, “Learning continuous control policies by stochastic value gradients,” in *Advances in Neural Information Processing Systems*, 2015, pp. 2944–2952.
- [17] P. Pilas, C. E. Rasmussen, J. Peters, and K. Doya, “Pipps: Flexible model-based policy search robust to the curse of chaos,” *arXiv preprint arXiv:1902.01240*, 2019.
- [18] Y. Mu, B. Peng, Z. Gu, S. E. Li, C. Liu, B. Nie, J. Zheng, and B. Zhang, “Mixed reinforcement learning for efficient policy optimization in stochastic environments,” in *2020 20th International Conference on Control, Automation and Systems (ICCAS)*. IEEE, 2020, pp. 1212–1219.
- [19] Y. Guan, S. E. Li, J. Duan, J. Li, Y. Ren, and B. Cheng, “Direct and indirect reinforcement learning,” *arXiv preprint arXiv:1912.10600*, 2019.
- [20] T. Degrif, M. White, and R. S. Sutton, “Off-policy actor-critic,” *arXiv preprint arXiv:1205.4839*, 2012.
- [21] J. Chen, X. Pan, R. Monga, S. Bengio, and R. Jozefowicz, “Revisiting distributed synchronous sgd,” *arXiv preprint arXiv:1604.00981*, 2016.
- [22] D.-A. Clevert, T. Unterthiner, and S. Hochreiter, “Fast and accurate deep network learning by exponential linear units (elus),” *arXiv preprint arXiv:1511.07289*, 2015.
- [23] D. P. Kingma and J. Ba, “Adam: A method for stochastic optimization,” *arXiv preprint arXiv:1412.6980*, 2014.
- [24] Y. Luo, H. Xu, Y. Li, Y. Tian, T. Darrell, and T. Ma, “Algorithmic framework for model-based deep reinforcement learning with theoretical guarantees,” *arXiv preprint arXiv:1807.03858*, 2018.
- [25] X. B. Peng, P. Abbeel, S. Levine, and M. van de Panne, “Deepmimic: Example-guided deep reinforcement learning of physics-based character skills,” *ACM Trans. Graph.*, vol. 37, no. 4, pp. 143:1–143:14, Jul. 2018. [Online]. Available: <http://doi.acm.org/10.1145/3197517.3201311>

## APPENDIX A PROOFS

### A. Chain rule

$$\begin{aligned}
& \nabla_{\hat{a}_t} \hat{r}_{t+k} \\
&= \begin{cases} \nabla_{\hat{s}_{t+k}} \hat{r}_{t+k} \prod_{j=k}^2 \nabla_{\hat{s}_{t+j-1}} \hat{s}_{t+j} \nabla_{\hat{a}_t} \hat{s}_{t+1}, & k \geq 2 \\ \nabla_{\hat{s}_{t+1}} \hat{r}_{t+1} \nabla_{\hat{a}_t} \hat{s}_{t+1}, & k = 1 \\ \nabla_{\hat{a}_t} \hat{r}_t, & k = 0 \end{cases} \\
& \nabla_{\hat{a}_t} r_{t+k} \\
&= \begin{cases} \nabla_{s_{t+k}} r_{t+k} \prod_{j=k}^2 \nabla_{s_{t+j-1}} s_{t+j} \nabla_{\hat{a}_t} s_{t+1}, & k \geq 2 \\ \nabla_{s_{t+1}} r_{t+1} \nabla_{\hat{a}_t} s_{t+1}, & k = 1 \\ \nabla_{\hat{a}_t} r_t, & k = 0 \end{cases} \\
& \nabla_{\hat{a}_t} \hat{Q}_{w,t+k} \\
&= \begin{cases} \nabla_{\hat{s}_{t+k}} \hat{Q}_{w,t+k} \prod_{j=k}^2 \nabla_{\hat{s}_{t+j-1}} \hat{s}_{t+j} \nabla_{\hat{a}_t} \hat{s}_{t+1}, & k \geq 2 \\ \nabla_{\hat{s}_{t+1}} \hat{Q}_{w,t+1} \nabla_{\hat{a}_t} \hat{s}_{t+1}, & k = 1 \\ \nabla_{\hat{a}_t} \hat{Q}_{w,t}, & k = 0 \end{cases} \\
& \nabla_{\hat{a}_t} q_{t+k}^{\pi_\theta} \\
&= \begin{cases} \nabla_{s_{t+k}} q_{t+k}^{\pi_\theta} \prod_{j=k}^2 \nabla_{s_{t+j-1}} s_{t+j} \nabla_{\hat{a}_t} s_{t+1}, & k \geq 2 \\ \nabla_{s_{t+1}} q_{t+1}^{\pi_\theta} \nabla_{\hat{a}_t} s_{t+1}, & k = 1 \\ \nabla_{\hat{a}_t} q_t^{\pi_\theta}, & k = 0 \end{cases}
\end{aligned}$$

### B. Proof of the Theorem 1

For simplicity, we denote

$$B_i^j := \mathbb{E}_{\substack{\hat{s}_{t+i}, \\ \dots, \\ \hat{s}_{t+n}}} \left\{ \sum_{l=t+i-1}^{t+j-1} \gamma^{l-t} \hat{r}_l + \gamma^j \hat{Q}_{w,t+j} \right\},$$

then

$$\begin{aligned}
& J_n^{\text{Model}}(\theta) \\
&= \mathbb{E}_{\hat{s}_t} \left\{ \nabla_\theta \mathbb{E}_{\substack{\hat{s}_{t+1}, \\ \dots, \\ \hat{s}_{t+n}}} \left\{ \sum_{l=t}^{n-1} \gamma^{l-t} \hat{r}_l + \gamma^n \hat{Q}_{w,t+n} \right\} \right\} \\
&= \mathbb{E}_{\hat{s}_t} \left\{ \nabla_{\hat{a}_t} B_1^n \nabla_\theta \pi_\theta + \mathbb{E}_{\hat{s}_{t+1}} \left\{ \nabla_{\hat{a}_{t+1}} B_2^n \nabla_\theta \pi_\theta \right\} + \dots \right\} \\
&= \sum_{k=0}^{n-1} \mathbb{E}_{\substack{\hat{s}_t, \\ \dots, \\ \hat{s}_{t+k}}} \left\{ \nabla_{\hat{a}_{t+k}} B_{k+1}^n \nabla_\theta \pi_\theta \right\} \\
&= \sum_{k=0}^{n-1} \mathbb{E}_{\hat{s}_{t+k} \sim \rho^{\pi_\theta}} \left\{ \nabla_{\hat{a}_{t+k}} B_{k+1}^n \nabla_\theta \pi_\theta \right\} \tag{a} \\
&= \sum_{k=0}^{n-1} \gamma^k \mathbb{E}_{\hat{s}_t} \left\{ \nabla_{\hat{a}_t} B_1^{n-k} \nabla_\theta \pi_\theta \right\} \\
&= \sum_{k=0}^{n-1} \gamma^k \nabla_\theta J_{n-k}(\theta) \tag{b}
\end{aligned}$$

where (a) is hold because of properties of stationary state distribution and  $f = p$ . Equation (b) is to substitute all  $\hat{s}_{t+k}, k = 0 : n-1$  with  $\hat{s}_t$  because they all have the same distribution  $\rho^{\pi_\theta}$ .

### C. Regular Conditions

#### Regular Conditions 1. (Continuity).

$$\begin{aligned}
& \nabla_s f(s, \pi_\theta(s)) \text{ is } L_{\nabla f}\text{-Lipschitz}, \\
& \nabla_s r(s, \pi_\theta(s)) \text{ is } L_{\nabla r}\text{-Lipschitz}, \\
& q^{\pi_\theta}(s, \pi_\theta(s)) \text{ is } L_q\text{-Lipschitz}, \\
& Q_w(s, \pi_\theta(s)) \text{ is } L_Q\text{-Lipschitz}, \\
& q^{\pi_\theta, o}(s, \pi_\theta(s)) \text{ is } L_{q^o}\text{-Lipschitz}, \\
& \nabla_s q^{\pi_\theta}(s, \pi_\theta(s)) \text{ is } L_{\nabla q}\text{-Lipschitz}, \\
& \nabla_s Q_w(s, \pi_\theta(s)) \text{ is } L_{\nabla Q}\text{-Lipschitz}, \\
& \nabla_s q^{\pi_\theta, o}(s, \pi_\theta(s)) \text{ is } L_{\nabla q^o}\text{-Lipschitz}.
\end{aligned}$$

#### Regular Conditions 2. (Boundedness).

$$\begin{aligned}
& \sup_{s \in \mathcal{S}, a \in \mathcal{A}} \|\delta(s, a)\| = B_\delta, \\
& \sup_{s \in \mathcal{S}} \|\nabla_s \delta(s, \pi(s))\| = B_{\nabla \delta s}, \\
& \sup_{s \in \mathcal{S}, a \in \mathcal{A}} \|\nabla_a \delta(s, a)\| = B_{\nabla \delta a}, \\
& \sup_{s \in \mathcal{S}} \|\nabla_s Q_w(s, \pi_\theta(s)) - \nabla_s q^{\pi_\theta, o}(s, \pi_\theta(s))\| = B_{qs}, \\
& \sup_{s \in \mathcal{S}, a \in \mathcal{A}} \|\nabla_a Q_w(s, a) - \nabla_a q^{\pi_\theta, o}(s, a)\| = B_{qa}, \\
& \sup_{s \in \mathcal{S}} \|\nabla_\theta \pi_\theta(s)\| = B_{\nabla \theta}, \\
& \sup_{j \geq 1} \sup_{s_t \in \mathcal{S}} \|\nabla_{s_t} f(s_{t+j}, \pi_\theta(s_{t+j}))\| = B_{\nabla fs}, \\
& \sup_{s \in \mathcal{S}, a \in \mathcal{A}} \|\nabla_a f(s, a)\| = B_{\nabla fa}, \\
& \sup_{j \geq 1} \sup_{s_t \in \mathcal{S}} \|\nabla_{s_t} p(s_{t+j}, \pi_\theta(s_{t+j}))\| = B_{\nabla ps}, \\
& \sup_{s \in \mathcal{S}, a \in \mathcal{A}} \|\nabla_a p(s, a)\| = B_{\nabla pa}, \\
& \sup_{s \in \mathcal{S}} \|\nabla_s r(s, \pi_\theta(s))\| = B_{\nabla rs}, \\
& \sup_{s \in \mathcal{S}, a \in \mathcal{A}} \|\nabla_a r(s, a)\| = B_{\nabla ra}, \\
& \sup_{s \in \mathcal{S}} \|\nabla_s q^{\pi_\theta}(s, \pi_\theta(s))\| = B_{\nabla qs}, \\
& \sup_{s \in \mathcal{S}, a \in \mathcal{A}} \|\nabla_s q^{\pi_\theta}(s, a)\| = B_{\nabla qa}, \\
& \sup_{s \in \mathcal{S}} \|\nabla_s Q_w(s, \pi_\theta(s))\| = B_{\nabla Qs}, \\
& \sup_{s \in \mathcal{S}, a \in \mathcal{A}} \|\nabla_a Q_w(s, a)\| = B_{\nabla Qa}, \\
& \sup_{s \in \mathcal{S}} \|\nabla_s q^{\pi_\theta, o}(s, \pi_\theta(s))\| = B_{\nabla q^o s}, \\
& \sup_{s \in \mathcal{S}, a \in \mathcal{A}} \|\nabla_a q^{\pi_\theta, o}(s, a)\| = B_{\nabla q^o a}
\end{aligned}$$

### D. Proof of Lemma 2

Inspired by the Lemma 4.3 of [24], which decomposed the difference of two value functions under different dynamics into a telescoping sum, we decompose the difference of two Q-value functions.

Denote  $q^{\pi_\theta, o}$  as the Q-value function under dynamics  $o$ . Let  $W_j$  be the cumulative reward when we use true dynamics  $p$  for  $j$  steps and then  $o$  for the rest of the steps, that is,

$$W_j = \mathbb{E}_{\substack{\forall t \geq 0, a_t = a \\ \forall 0 \leq t < j, s_{t+1} \sim p(\cdot | s_t, a_t) \\ \forall t \geq j, s_{t+1} \sim o(\cdot | s_t, a_t)}} \left\{ \sum_{t=0}^{\infty} \gamma^t r_t \middle| s_0 = s \right\},$$

then we have  $W_0 = q^{\pi_\theta, o}(s, a)$  and  $W_\infty = q^{\pi_\theta}(s, a)$ ,

$$q^{\pi_\theta}(s, a) - q^{\pi_\theta, o}(s, a) = \sum_{j=0}^{\infty} (W_{j+1} - W_j)$$

where

$$\begin{aligned} W_j &= R + \mathbb{E}_{s_j \sim \pi_\theta, p} \left\{ \mathbb{E}_{s_{j+1} \sim o(\cdot | s_j, \pi_\theta(s_j))} \left\{ \gamma^{j+1} q_{s_{j+1}}^{\pi_\theta, o} \right\} \right\} \\ W_{j+1} &= R + \mathbb{E}_{s_j \sim \pi_\theta, p} \left\{ \mathbb{E}_{s_{j+1} \sim p(\cdot | s_j, \pi_\theta(s_j))} \left\{ \gamma^{j+1} q_{s_{j+1}}^{\pi_\theta, o} \right\} \right\}, \end{aligned}$$

in which  $R$  is expected accumulative reward of the first  $j$  steps from policy  $\pi$  and true dynamics  $p$ ,  $q_s^{\pi_\theta, o} := q^{\pi_\theta, o}(s, \pi_\theta(s))$ . In our case,

$$\begin{aligned} q^{\pi_\theta}(s, a) - q^{\pi_\theta, o}(s, a) &= \sum_{j=0}^{\infty} (W_{j+1} - W_j) \\ &= \sum_{j=0}^{\infty} \gamma^{j+1} (q_{s_{j+1}}^{\pi_\theta, o} - \mathbb{E}_\epsilon \left\{ q_{s_{j+1}+\epsilon}^{\pi_\theta, o} \right\}), \end{aligned}$$

so the upper bound can be derived as follows,

$$\begin{aligned} &\sup_{s \in \mathcal{S}} \|\nabla_s q^{\pi_\theta}(s, \pi_\theta(s)) - \nabla_s q^{\pi_\theta, o}(s, \pi_\theta(s))\| \\ &\leq \sum_{j=0}^{\infty} \gamma^{j+1} \mathbb{E}_\epsilon \left\{ \sup_{s \in \mathcal{S}} \|\nabla_s q_{s_{j+1}}^{\pi_\theta, o} - \nabla_s q_{s_{j+1}+\epsilon}^{\pi_\theta, o}\| \right\} \\ &\leq \sum_{j=0}^{\infty} \gamma^{j+1} \mathbb{E}_\epsilon \left\{ L_{\nabla q^o} \|\epsilon\| B_{\nabla ps} \right\} \quad (13) \\ &= \frac{\gamma}{1-\gamma} L_{\nabla q^o} B_{\nabla ps} \mathbb{E}_\epsilon \left\{ \|\epsilon\| \right\} = c_{d1} \mathbb{E}_\epsilon \left\{ \|\epsilon\| \right\}, \end{aligned}$$

where  $c_{d1} = \frac{\gamma}{1-\gamma} L_{\nabla q^o} B_{\nabla ps}$ , and (13) requires the continuity condition of  $\nabla_s q^{\pi_\theta, o}$  and the boundedness condition of the gradient through the state chain.

$$\begin{aligned} &\sup_{s \in \mathcal{S}, a \in \mathcal{A}} \|\nabla_a q^{\pi_\theta}(s, a) - \nabla_a q^{\pi_\theta, o}(s, a)\| \\ &\leq \sum_{j=0}^{\infty} \gamma^{j+1} \mathbb{E}_\epsilon \left\{ \sup_{s \in \mathcal{S}, a \in \mathcal{A}} \|\nabla_a q_{s_{j+1}}^{\pi_\theta, o} - \nabla_a q_{s_{j+1}+\epsilon}^{\pi_\theta, o}\| \right\} \\ &\leq \sum_{j=0}^{\infty} \gamma^{j+1} \mathbb{E}_\epsilon \left\{ L_{\nabla q^o} \|\epsilon\| B_{\nabla ps} B_{\nabla pa} \right\} \quad (14) \\ &= \frac{\gamma}{1-\gamma} L_{\nabla q^o} B_{\nabla ps} B_{\nabla pa} \mathbb{E}_\epsilon \left\{ \|\epsilon\| \right\} = c_{d2} \mathbb{E}_\epsilon \left\{ \|\epsilon\| \right\}, \end{aligned}$$

where  $c_{d2} = \frac{\gamma}{1-\gamma} L_{\nabla q^o} B_{\nabla ps} B_{\nabla pa}$ . Besides the conditions required by (13), (14) also requires the boundedness of  $p$ 's derivative w.r.t.  $a$ .

### E. Proof of Lemma 3

We denote  $\Delta_{s, t+i} := \sup_{\hat{s}_t \in \mathcal{S}, \hat{a}_t \in \mathcal{A}} \|\hat{s}_{t+i} - s_{t+i}\|$ , and  $\Delta_{\nabla s, t+i} := \sup_{\hat{s}_t \in \mathcal{S}, \hat{a}_t \in \mathcal{A}} \|\nabla_{\hat{s}_{t+i}} \hat{s}_{t+i+1} - \nabla_{s_{t+i}} s_{t+i+1}\|$ . From the regular conditions from Appendix A-C, we have

$$\begin{aligned} &\Delta_{\nabla s, t+i} \\ &\leq \sup_{\hat{s}_t \in \mathcal{S}, \hat{a}_t \in \mathcal{A}} \|\nabla_{\hat{s}_{t+i}} \hat{s}_{t+i+1} - \nabla_{s_{t+i}} \hat{s}_{t+i+1} + \nabla_{s_{t+i}} \hat{s}_{t+i+1} - \nabla_{s_{t+i}} s_{t+i+1}\| \\ &\leq L_{\nabla f} \sup_{\hat{s}_t \in \mathcal{S}, \hat{a}_t \in \mathcal{A}} \|\hat{s}_{t+i} - s_{t+i}\| + B_{\nabla \delta s} \\ &= L_{\nabla f} \Delta_{s, t+i} + B_{\nabla \delta s}, i \geq 0. \end{aligned}$$

Then, we will discuss the upper bound in three cases:  $k \geq 2$ ,  $k = 1$  and  $k = 0$ .

$$\text{Case} \quad 1: \quad k \quad \geq \quad 2$$

$$\begin{aligned} &\sup_{\hat{s}_t \in \mathcal{S}, \hat{a}_t \in \mathcal{A}} \|\nabla_{\hat{a}_t} \hat{r}_{t+k} - \nabla_{\hat{a}_t} r_{t+k}\| \\ &= \sup_{\hat{s}_t \in \mathcal{S}, \hat{a}_t \in \mathcal{A}} \|\nabla_{\hat{a}_t} \hat{r}_{t+k} - \nabla_{s_{t+k}} r_{t+k} \prod_{j=k}^2 \nabla_{\hat{s}_{t+j-1}} \hat{s}_{t+j} \nabla_{\hat{a}_t} \hat{s}_{t+1} + \nabla_{s_{t+k}} r_{t+k} \prod_{j=k}^2 \nabla_{\hat{s}_{t+j-1}} \hat{s}_{t+j} \nabla_{\hat{a}_t} \hat{s}_{t+1} - \nabla_{\hat{a}_t} r_{t+k}\| \\ &\leq L_{\nabla r} \sup_{\hat{s}_t \in \mathcal{S}, \hat{a}_t \in \mathcal{A}} \|\hat{s}_{t+k} - s_{t+k}\| B_{\nabla fs} B_{\nabla fa} + \sup_{\hat{s}_t \in \mathcal{S}, \hat{a}_t \in \mathcal{A}} B_{\nabla rs} \|\prod_{j=k}^2 \nabla_{\hat{s}_{t+j-1}} \hat{s}_{t+j} \nabla_{\hat{a}_t} \hat{s}_{t+1} - \prod_{j=k}^2 \nabla_{s_{t+j-1}} s_{t+j} \nabla_{\hat{a}_t} s_{t+1}\| \\ &= L_{\nabla r} \Delta_{s, t+k} B_{\nabla fs} B_{\nabla fa} + \sup_{\hat{s}_t \in \mathcal{S}, \hat{a}_t \in \mathcal{A}} B_{\nabla rs} \|\prod_{j=k}^2 \nabla_{\hat{s}_{t+j-1}} \hat{s}_{t+j} \nabla_{\hat{a}_t} \hat{s}_{t+1} - \prod_{j=k}^2 \nabla_{\hat{s}_{t+j-1}} \hat{s}_{t+j} \nabla_{\hat{a}_t} s_{t+1} + \prod_{j=k}^2 \nabla_{\hat{s}_{t+j-1}} \hat{s}_{t+j} \nabla_{\hat{a}_t} s_{t+1} - \prod_{j=k}^2 \nabla_{s_{t+j-1}} s_{t+j} \nabla_{\hat{a}_t} s_{t+1}\| \\ &\leq L_{\nabla r} \Delta_{s, t+k} B_{\nabla fs} B_{\nabla fa} + B_{\nabla rs} \left( B_{\nabla fs} B_{\nabla \delta a} + B_{\nabla pa} \prod_{j=k}^2 ((\nabla_{\hat{s}_{t+j-1}} \hat{s}_{t+j} - \nabla_{s_{t+j-1}} s_{t+j}) + \nabla_{s_{t+j-1}} s_{t+j}) - \prod_{j=k}^2 \nabla_{s_{t+j-1}} s_{t+j} \right) \\ &\leq L_{\nabla r} \Delta_{s, t+k} B_{\nabla fs} B_{\nabla fa} + B_{\nabla rs} \left( B_{\nabla fs} B_{\nabla \delta a} + B_{\nabla pa} \sum_{j=1}^{k-1} C_{k-1}^j \max_{1 < i \leq k} \Delta_{\nabla s, t+i-1}^j B_{\nabla ps}^{k-1-j} \right) \\ &\leq L_{\nabla r} B_{\nabla fs} B_{\nabla fa} c_m k + B_{\nabla rs} B_{\nabla fs} B_{\nabla \delta a} + B_{\nabla rs} B_{\nabla pa} \sum_{j=1}^{k-1} C_{k-1}^j B_{\nabla ps}^{k-1-j} (L_{\nabla f} c_m (k-1) + B_{\nabla \delta s})^j \\ &\leq L_{\nabla r} B_{\nabla fs} B_{\nabla fa} c_m k + B_{\nabla rs} B_{\nabla fs} B_{\nabla \delta a} + B_{\nabla rs} B_{\nabla pa} B_{\nabla ps}^{k-1} ((L_{\nabla f} c_m (k-1) + B_{\nabla \delta s}) / B_{\nabla ps})^{(k-1)} = o((c_m k)^k) = U_r(k) \end{aligned}$$

$$\begin{aligned}
& \sup_{\hat{s}_t \in \mathcal{S}, \hat{a}_t \in \mathcal{A}} \|\nabla_{\hat{a}_t} \hat{Q}_{w,t+k} - \nabla_{\hat{a}_t} q_{t+k}^{\pi_\theta}\| \\
& \leq \sup_{\hat{s}_t \in \mathcal{S}, \hat{a}_t \in \mathcal{A}} \|\nabla_{\hat{a}_t} \hat{Q}_{w,t+k} - \nabla_{\hat{a}_t} Q_{w,t+k} + \\
& \quad \nabla_{\hat{a}_t} Q_{w,t+k} - \nabla_{\hat{a}_t} q_{t+k}^{\pi_\theta}\| \\
& \leq \sup_{\hat{s}_t \in \mathcal{S}, \hat{a}_t \in \mathcal{A}} \|\nabla_{\hat{a}_t} \hat{Q}_{w,t+k} - \nabla_{\hat{a}_t} Q_{w,t+k}\| + \\
& \quad \sup_{\hat{s}_t \in \mathcal{S}, \hat{a}_t \in \mathcal{A}} \|\nabla_{s_{t+k}} Q_{w,t+k} - \nabla_{s_{t+k}} q_{t+k}^{\pi_\theta}\| B_{\nabla pa} B_{\nabla ps} \\
& \leq o((c_m k)^k) + \left( \sup_{\hat{s}_t \in \mathcal{S}, \hat{a}_t \in \mathcal{A}} \|\nabla_{s_{t+k}} Q_{w,t+k} - \nabla_{s_{t+k}} q_{t+k}^{\pi_\theta, o}\| + \right. \\
& \quad \left. \sup_{\hat{s}_t \in \mathcal{S}, \hat{a}_t \in \mathcal{A}} \|\nabla_{s_{t+k}} q_{t+k}^{\pi_\theta, o} - \nabla_{s_{t+k}} q_{t+k}^{\pi_\theta}\| \right) B_{\nabla pa} B_{\nabla ps} \\
& \leq o((c_m k)^k) + B_{qs} B_{\nabla pa} B_{\nabla ps} + c_{d1} \mathbb{E}_\epsilon \{\|\epsilon\|\} B_{\nabla pa} B_{\nabla ps} \\
& = o((c_m k)^k) + \text{const} \cdot (B_{qs} + \mathbb{E}_\epsilon \{\|\epsilon\|\}) \\
& = U_q(k)
\end{aligned}$$

Case 2:  $k = 1$

$$\begin{aligned}
& \sup_{\hat{s}_t \in \mathcal{S}, \hat{a}_t \in \mathcal{A}} \|\nabla_{\hat{a}_t} \hat{r}_{t+1} - \nabla_{\hat{a}_t} r_{t+1}\| \\
& = \sup_{\hat{s}_t \in \mathcal{S}, \hat{a}_t \in \mathcal{A}} \|\nabla_{\hat{s}_{t+1}} \hat{r}_{t+1} \nabla_{\hat{a}_t} \hat{s}_{t+1} - \nabla_{s_{t+1}} r_{t+1} \nabla_{\hat{a}_t} s_{t+1}\| \\
& = \sup_{\hat{s}_t \in \mathcal{S}, \hat{a}_t \in \mathcal{A}} \|\nabla_{\hat{s}_{t+1}} \hat{r}_{t+1} \nabla_{\hat{a}_t} \hat{s}_{t+1} - \nabla_{s_{t+1}} r_{t+1} \nabla_{\hat{a}_t} \hat{s}_{t+1} + \\
& \quad \nabla_{s_{t+1}} r_{t+1} \nabla_{\hat{a}_t} \hat{s}_{t+1} - \nabla_{s_{t+1}} r_{t+1} \nabla_{\hat{a}_t} s_{t+1}\| \\
& \leq L_{\nabla r} \sup_{\hat{s}_t \in \mathcal{S}, \hat{a}_t \in \mathcal{A}} \|\hat{s}_{t+1} - s_{t+1}\| B_{\nabla fa} + B_{\nabla rs} B_{\nabla \delta a} \\
& \leq L_{\nabla r} B_{\nabla fa} c_m + B_{\nabla rs} B_{\nabla \delta a} \\
& = U_r(1)
\end{aligned}$$

$$\begin{aligned}
& \sup_{\hat{s}_t \in \mathcal{S}, \hat{a}_t \in \mathcal{A}} \|\nabla_{\hat{a}_t} \hat{Q}_{w,t+1} - \nabla_{\hat{a}_t} q_{t+1}^{\pi_\theta}\| \\
& \leq \sup_{\hat{s}_t \in \mathcal{S}, \hat{a}_t \in \mathcal{A}} \|\nabla_{\hat{a}_t} \hat{Q}_{w,t+1} - \nabla_{\hat{a}_t} Q_{w,t+1} + \\
& \quad \nabla_{\hat{a}_t} Q_{w,t+1} - \nabla_{\hat{a}_t} q_{t+1}^{\pi_\theta}\| \\
& \leq L_{\nabla Q} B_{\nabla fa} c_m + B_{\nabla Qs} B_{\nabla \delta a} + \\
& \quad \sup_{\hat{s}_t \in \mathcal{S}, \hat{a}_t \in \mathcal{A}} \|\nabla_{\hat{a}_t} Q_{w,t+1} - \nabla_{\hat{a}_t} q_{t+1}^{\pi_\theta, o}\| + \\
& \quad \sup_{\hat{s}_t \in \mathcal{S}, \hat{a}_t \in \mathcal{A}} \|\nabla_{\hat{a}_t} q_{t+1}^{\pi_\theta, o} - \nabla_{\hat{a}_t} q_{t+1}^{\pi_\theta}\| \\
& \leq L_{\nabla Q} B_{\nabla fa} c_m + B_{\nabla Qs} B_{\nabla \delta a} + B_{qs} B_{\nabla pa} + c_{d2} \mathbb{E}_\epsilon \{\|\epsilon\|\} \\
& = U_q(1)
\end{aligned}$$

Case 3:  $k = 0$

$$\begin{aligned}
& \sup_{\hat{s}_t \in \mathcal{S}, \hat{a}_t \in \mathcal{A}} \|\nabla_{\hat{a}_t} \hat{r}_t - \nabla_{\hat{a}_t} r_t\| \\
& = 0 = U_r(0)
\end{aligned}$$

$$\begin{aligned}
& \sup_{\hat{s}_t \in \mathcal{S}, \hat{a}_t \in \mathcal{A}} \|\nabla_{\hat{a}_t} \hat{Q}_{w,t} - \nabla_{\hat{a}_t} q_t^{\pi_\theta}\| \\
& \leq \sup_{\hat{s}_t \in \mathcal{S}, \hat{a}_t \in \mathcal{A}} \|\nabla_{\hat{a}_t} \hat{Q}_{w,t} - \nabla_{\hat{a}_t} q_t^{\pi_\theta, o}\| + \\
& \quad \sup_{\hat{s}_t \in \mathcal{S}, \hat{a}_t \in \mathcal{A}} \|\nabla_{\hat{a}_t} q_t^{\pi_\theta, o} - \nabla_{\hat{a}_t} q_t^{\pi_\theta}\| \\
& \leq B_{qa} + c_{d2} \mathbb{E}_\epsilon \{\|\epsilon\|\} = U_q(0)
\end{aligned}$$

### F. Proof of Theorem 2

For simplicity, we denote

$$D_n(\hat{s}_t, \hat{a}_t) = \sum_{l=t}^{n-1+t} \gamma^{l-t} (\hat{r}_l - r_l) + \gamma^n (\hat{Q}_{w,t+n} - q_{t+n}^{\pi_\theta}),$$

then

$$\begin{aligned}
& \sup \|\nabla_{\hat{a}_t} D_n(\hat{s}_t, \hat{a}_t) \mid_{\hat{a}_t = \pi_\theta(\hat{s}_t)}\| \\
& = \left\| \sum_{l=t}^{n-1+t} \gamma^{l-t} (\nabla_{\hat{a}_t} \hat{r}_l - \nabla_{\hat{a}_t} r_l) + \gamma^n (\nabla_{\hat{a}_t} \hat{Q}_{w,t+n} - \nabla_{\hat{a}_t} q_{t+n}^{\pi_\theta}) \right\| \\
& \leq \sum_{l=t}^{n-1+t} \gamma^{l-t} \sup \|\nabla_{\hat{a}_t} \hat{r}_l - \nabla_{\hat{a}_t} r_l\| + \gamma^n \sup \|\nabla_{\hat{a}_t} \hat{Q}_{w,t+n} - \nabla_{\hat{a}_t} q_{t+n}^{\pi_\theta}\| \\
& \leq \sum_{k=0}^{n-1} \gamma^k U_r(k) + \gamma^n U_q(n)
\end{aligned}$$

Finally,

$$\begin{aligned}
& \|\nabla_\theta J_n(\theta) - \nabla_\theta J(\theta)\| \\
& \leq \mathbb{E}_{\hat{s}_t} \left\{ \left\| \nabla_{\hat{a}_t} D_n(\hat{s}_t, \hat{a}_t) \right\|_{\hat{a}_t = \pi_\theta(\hat{s}_t)} \nabla_\theta \pi_\theta(\hat{s}_t) \right\} \\
& \leq \mathbb{E}_{\hat{s}_t} \left\{ \left\| \nabla_{\hat{a}_t} D_n(\hat{s}_t, \hat{a}_t) \right\|_{\hat{a}_t = \pi_\theta(\hat{s}_t)} \right\} \left\| \nabla_\theta \pi_\theta(\hat{s}_t) \right\| \\
& \leq B_{\nabla \theta} \left( \sum_{k=0}^{n-1} \gamma^k U_r(k) + \gamma^n U_q(n) \right) \\
& \leq \begin{cases} o(n(\gamma c_m n)^n) + \gamma^n \text{const} \cdot (B_{qs} + \mathbb{E}_\epsilon \{\|\epsilon\|\}), & n \geq 1 \\ \text{const} \cdot (B_{qa} + \mathbb{E}_\epsilon \{\|\epsilon\|\}), & n = 0 \end{cases}
\end{aligned}$$

## APPENDIX B TASKS FORMULATION

### A. Path tracking task

We have developed a simulator for the learning of data-driven algorithms in the path tracking task, in which a reference path and a desired velocity are given for the vehicle to track in 2-dimensional coordination. The reference path is the composition of three sine curves with different magnitudes and periods, specifically,

$$y_{\text{ref}} = 7.5 \sin \frac{2\pi x}{200} + 2.5 \sin \frac{2\pi x}{300} - 5 \sin \frac{2\pi x}{400}$$

where  $y_{\text{ref}}$  corresponds to a reference lateral position in  $x$ . Besides, we can easily calculate the reference angle  $\phi_{\text{ref}}$  by the slope of each reference point. The desired velocity  $u_{\text{ref}}$  is set to be 20m/s.

The bicycle model and linear tire model are used as our vehicle model, in which the vehicle states and control inputs of this problem are listed in Table II, and the vehicle parameters are listed in Table III. The vehicle is controlled by a saturating actuator, where  $\delta \in [-0.4, 0.4]$  and  $acc \in [-3, 3]$ . We use the first order backward Euler method to discretize the model. Note that the system frequency  $f_{\text{sys}}$  used for simulation is

different from the sampling frequency  $f_{\text{sam}}$ . The discretized vehicle dynamics are:

$$s^{\text{veh}} = \begin{bmatrix} u \\ v \\ r \\ y \\ \phi \\ x \end{bmatrix}, a^{\text{veh}} = \begin{bmatrix} \delta \\ acc \end{bmatrix}, T = \frac{1}{f_{\text{sys}}},$$

$$s_{k+1}^{\text{veh}} = f(s_k^{\text{veh}}, a_k^{\text{veh}}) \quad (15)$$

$$= \begin{bmatrix} u_k + T(acc_k + v_k r_k) \\ mv_k u_k + T(aC_f - bC_r)r_k - TC_f \delta_k u_k - Tmu_k^2 r_k \\ mu_k - T(C_f + C_r) \\ -I_z r_k u_k - T(aC_f - bC_r)v_k + TaC_f \delta_k u_k \\ y_k + T(u_k \sin \phi_k + v_k \cos \phi_k) \\ \phi_k + Tr_k \\ x_k + T(u_k \cos \phi_k - v_k \sin \phi_k) \end{bmatrix}$$

With the reference path and vehicle states, the state and action spaces for RL learning can be constructed, in which states and actions are represented as

$$s = [\delta_u, v, r, \delta_y, \delta_\phi, x]^\top \in \mathcal{S},$$

$$a = [\delta, acc]^\top \in \mathcal{A},$$

where  $\delta_u = u - u_{\text{ref}}$  is the speed deviation,  $\delta_y = y - y_{\text{ref}}$  is the distance between the vehicle center of gravity (CG) and the reference path,  $\delta_\phi = \phi - \phi_{\text{ref}}$  is the yaw angle between the vehicle and the reference path. Finally, we get a 6-dimensional state space and a 2-dimensional action space.

The reward function is designed to minimize tracking errors, as shown below,

$$r(s, a) = -0.01\delta_u^2 - 0.04\delta_y^2 - 0.1\delta_\phi^2 - 0.02r^2 - 5\delta^2 - 0.05acc^2 \quad (16)$$

The state is initialized randomly to add diversity of the task. Besides, to enhance sample efficiency, the simulator is designed to simulate in parallel, in which a hyperparameter  $N_{\text{agent}}$  controls the number of agents that work simultaneously. To cut meaningless samples, early termination technology is also adopted by the simulator, as does in [25]. The simulation will be reset when the vehicle deviates too much from the reference path or loses stability. Specifically, the terminal state set is  $\mathcal{S}_T = \{s | s \in \mathcal{S}, \delta_y > 3 \text{ or } \delta_\phi > \pi/4 \text{ or } u < 2 \text{ or } r > 0.8\}$ .

Compared with the simulator, we make three changes in the model. First, the vehicle in the prior model is controlled to track a straight line, i.e., the x-axis, instead of the composition of several sine curves. Then, we add a biased Gaussian noise in the dimension of  $y$ . Finally, the sample frequency is directly used in the discretization of the model. The prior model is shown as follows,

$$y_{\text{ref}} = \phi_{\text{ref}} = 0, T = \frac{1}{f_{\text{sam}}},$$

$$\hat{s}_{k+1}^{\text{veh}} = f(\hat{s}_k^{\text{veh}}, \hat{a}_k^{\text{veh}}) + [0, 0, 0, \mathcal{N}(0.5, 0.01), 0, 0]^\top \quad (17)$$

Similar to the simulator, the state  $\hat{s}$  and action  $\hat{a}$  can be constructed accordingly. Besides, the reward function in the prior model is the same as that in the simulator.

For the minimum return to work in the task, we first choose a tolerable value of each state during a episode, i.e.,  $\delta_u^2 =$

TABLE II: VEHICLE STATES AND CONTROL INPUTS

Variable	Meaning	Unit
$u$	Longitudinal velocity	[m/s]
$v$	Lateral velocity	[m/s]
$r$	Yaw rate at center of gravity (CG)	[rad/s]
$x$	X coordinate	[m]
$y$	Y coordinate	[m]
$\phi$	Yaw angle	[rad]
$\delta$	Front wheel angle	[rad]
$acc$	Longitudinal acceleration	[m/s <sup>2</sup> ]

TABLE III: VEHICLE PARAMETERS

Parameter	Meaning	Value
$C_f$	Front wheel cornering stiffness	-88000 [N/rad]
$C_r$	Rear wheel cornering stiffness	-94000 [N/rad]
$a$	Distance from CG to front axle	1.14 [m]
$b$	Distance from CG to rear axle	1.40 [m]
$m$	Mass	1500 [kg]
$I_z$	Polar moment of inertia at CG	2420 [kg·m <sup>2</sup> ]
$\mu$	Tire-road friction coefficient	1.0
$f_{\text{sam}}$	Sampling frequency	10 [Hz]
$f_{\text{sys}}$	System frequency	200 [Hz]

2,  $\delta_y^2 = 1$ ,  $\delta_\phi^2 = \pi/18$ ,  $r = 0.2$ ,  $\delta = 0.1$ ,  $acc = 0.5$ , to compute a tolerable reward using (16). Then the minimum return equals the reward times the episode length 200.

### B. Inverted pendulum task

We adapted the inverted pendulum task in the Gym package by only changing its reward function while the state and action remain the same, as shown below,

$$s = [x, \theta, \dot{x}, \dot{\theta}]^\top \in \mathcal{S},$$

$$a = [F]^\top \in \mathcal{A},$$

where  $x$  and  $\dot{x}$  are position and velocity of the cart,  $\theta$  and  $\dot{\theta}$  are the angle and angular velocity of the pole, and  $F$  is the force applied to the cart.

The reward function is designed as below,

$$r(s, a) = -0.01x^2 - \theta^2 - 0.1\dot{x}^2 - 0.1\dot{\theta}^2. \quad (18)$$

The true dynamics is not explicit in the MuJoCo. We first construct the model by the rigid body dynamics. Denote  $y = [x, \theta]^\top$ , then  $s = [y^\top, \dot{y}^\top]^\top$ ,

$$s_{k+1} = f(s_k, a_k) = \begin{bmatrix} y_k + Ty_k \\ \dot{y}_k + TD^{-1}z \end{bmatrix}, T = \frac{1}{f_{\text{sam}}},$$

$$D = \begin{bmatrix} m_1 + m_2 & (m_1/2 + m_2)l \cos \theta \\ (m_1/2 + m_2)l \cos \theta & (m_1/3 + m_2)l/2 \end{bmatrix},$$

$$z = \begin{bmatrix} (m_1/2 + m_2)l\dot{\theta}^2 \sin \theta + F \\ (m_1/2 + m_2)lg \sin \theta \end{bmatrix}$$

where all the parameters are shown in Table IV. We then add a biased noise in the first dimension to construct the prior model of this task, i.e.,

$$\hat{s}_{k+1} = f(\hat{s}_k, \hat{a}_k) + [\mathcal{N}(0.1, 0.5), 0, 0, 0]^\top.$$

Besides, the reward function in the model is modified as

$$\hat{r}(\hat{s}, \hat{a}) = -0.01\hat{x}^2 - \hat{\theta}^2 - 0.001\hat{x}^2 - 0.001\hat{\theta}^2.$$

TABLE IV: PARAMETERS FOR INVERTED PENDULUM TASK

Parameter	Meaning	Value
$m_1$	Mass of the cart	9.42 [Kg]
$m_2$	Mass of the pole	4.89 [Kg]
$l$	Length of the pole	0.6 [m]
$g$	Acceleration of gravity	9.81 [ $\text{m}^2/\text{s}$ ]
$f_{\text{sam}}$	Sampling frequency	25 [Hz]
$f_{\text{sys}}$	System frequency	50 [Hz]

It can be seen that the model mismatch comes from three aspects. The first is in the transition model  $f$ , which is constructed without considering friction, damping in the joints or contact force compared with the true dynamics in the MuJoCo. Besides, it uses a different numerical integrator and contains the biased noise. The second is the different discrete time steps. And the last one is the reward function.

For the minimum return to work in the task, we first choose a tolerable value of each state during an episode, i.e.,  $x = 2, \theta = 0.1, \dot{x} = 0.1, \dot{\theta} = 0.05$ , to compute a tolerable reward using (18). Then the minimum return equals the reward times the episode length 100.

### APPENDIX C ADDITIONAL DESCRIPTIONS

#### A. General form of MPG

The general form of the MPG is as follows,

$$\nabla_{\theta} J^{\text{Mixed}} = \sum_{i \in \mathbb{I}} w_i \nabla_{\theta} J_i(\theta),$$

where  $\mathbb{I}$  is the set of used horizon lengths,  $\mathbb{I} \subset \mathbb{N}$  and  $0 \in \mathbb{I}$ , and  $w_i (i \in \mathbb{I})$  are the weights to be determined. A corresponding rule-based weighting method is

$$w_i = \text{Softmax}(1/\text{Rule-Error}_i), i \in \mathbb{I}$$

$$\text{Rule-Error}_i = \begin{cases} \lambda^i, & \lambda \leq 1 \\ (2 - \lambda)^{\max \mathbb{I} - i}, & \lambda > 1 \end{cases},$$

where  $\lambda$  is a variable that linearly increases from  $1 - \eta$  to  $1 + \eta$  within iteration  $T$  and remains  $1 + \eta$  thereafter,  $\eta \in (0, 1)$  and  $T$  are served as hyperparameters.

#### B. Basic description of the algorithms

See Table V.

TABLE V: BASIC DESCRIPTION OF THE ALGORITHMS.

Algorithm	D/S*	Value target	PG	Info source
MPG-v1	D	$n$ -step TD	MPG	Data & model
MPG-v2	D	Clipped double Q	MPG	Data & model
$n$ -step DPG	D	$n$ -step TD	DPG	Data
$n$ -step ADP	D	$n$ -step TD	Model PG	Model
TD3	D	Clipped double Q	DPG	Data
SAC	S	Clipped double Q	Soft PG	Data

\* Deterministic policy or Stochastic policy.

TABLE VI: DETAILED HYPERPARAMETERS.

Algorithm	Value
<i>Shared</i>	
Optimizer	Adam ( $\beta_1 = 0.9, \beta_2 = 0.999$ )
Approximation function	MLP
Number of hidden layers	2
Number of hidden units	256
Nonlinearity of hidden layer	ELU
Replay buffer size	5e5
Batch size	256
Policy learning rate	Linear decay 3e-4 $\rightarrow$ 3e-6
Value learning rate	Linear decay 8e-4 $\rightarrow$ 8e-6
Discount factor $\gamma$	0.98
Target smoothing coefficient $\tau$	0.005
Number of Actors	2
Number of Buffers	2
Number of Learners	12
<i>MPG (v1, v2)</i>	
Weighting schedule $\eta, T$	0.1, 9000/4000*
$H$	25
$n$ for value/policy learning	25
Number batch reuse	10
Delayed update	2
<i>n-step DPG, n-step ADP</i>	
$n$ for value/policy learning	25
Number batch reuse	10
<i>TD3</i>	
Exploration noise	$\epsilon \sim \mathcal{N}(0, 0.1)$
Delayed update	2
Policy smoothing noise	$\epsilon \sim \text{clip}(\mathcal{N}(0, 0.1), -0.5, 0.5)$
<i>SAC</i>	
Fixed $\alpha$	0.03

\* For path tracking and inverted pendulum tasks, respectively.

### C. Hyperparameters

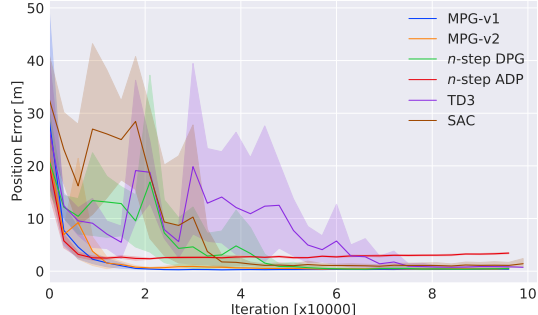
See Table VI.

### APPENDIX D ADDITIONAL RESULTS

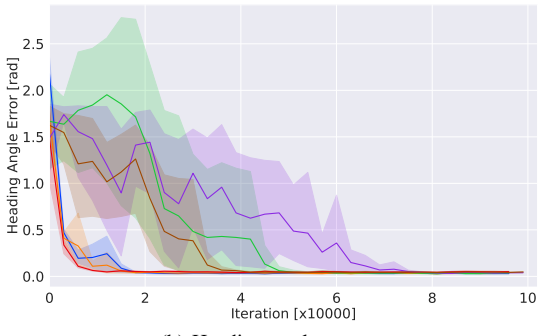
Fig. 7 graphs the tracking errors of all baseline algorithms on the path tracking task. We calculate the tracking errors using the root mean squared over states of 5 episodes every 3000 iterations (each episode has a fixed length of 200). Specifically, the errors are calculated by

$$\text{Error}_{\dagger} = \sqrt{\mathbb{E}_{\dagger \in \mathbb{C}_{\dagger}} \{(\dagger - \dagger_{\text{ref}})^2\}}$$

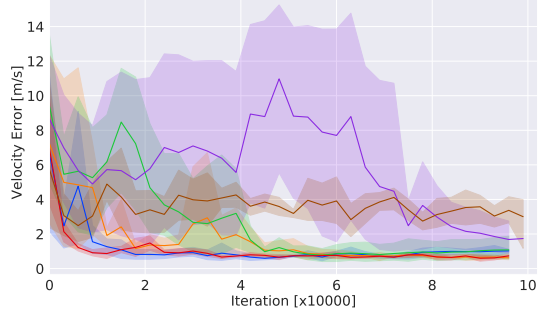
where  $\text{Error}_{\dagger}, \dagger \in \{y, \phi, u\}$  is to denote the position error, heading angle error and velocity error, respectively.  $\mathbb{C}_{\dagger}$  is the corresponding state collection of 5 episodes.



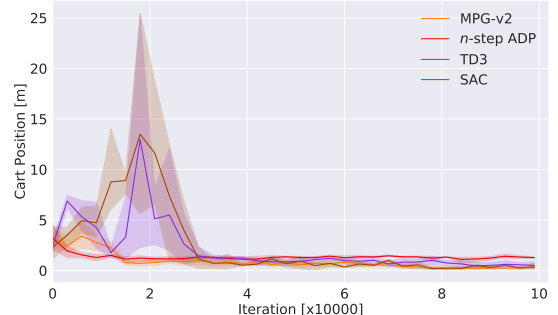
(a) Position error



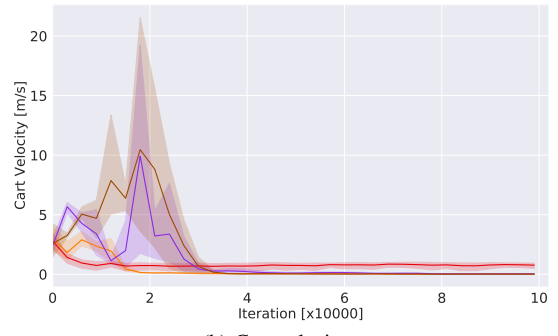
(b) Heading angle error



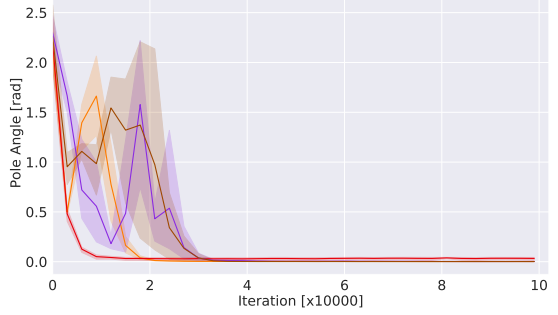
(c) Velocity error



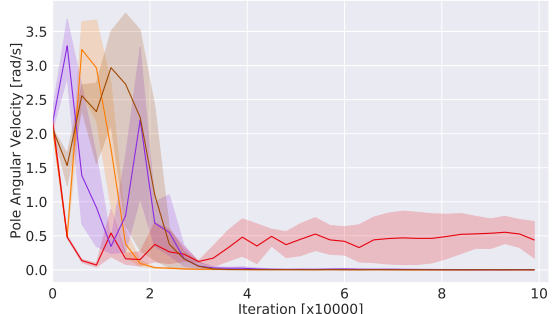
(a) Cart position



(b) Cart velocity



(c) Pole angle



(d) Pole angular velocity

Fig. 7: Tracking errors of path tracking task. (a) Position error. (b) Heading angle error. (c) Velocity error. The solid lines correspond to the mean and the shaded regions correspond to 95% confidence interval over 5 runs.

Besides, Fig. 8 graphs the state magnitudes on the inverted pendulum task, which is calculated by the root mean square over actions of 5 episodes every 3000 iterations. Specifically, the state magnitudes are calculated by

$$\text{State}_{\dagger} = \sqrt{\mathbb{E}_{\dagger \in \mathbb{C}_{\dagger}} \{\dagger^2\}}$$

where  $\text{State}_{\dagger}, \dagger \in \{x, \dot{x}, \theta, \dot{\theta}\}$  is to denote the magnitude of the cart position, cart velocity, pole angle and pole angular velocity, respectively.  $\mathbb{C}_{\dagger}$  is the corresponding state collection of 5 episodes.

Fig. 8: State magnitudes of inverted pendulum task. (a) Cart position. (b) Cart velocity. (c) Pole angle. (d) Pole angular velocity. The solid lines correspond to the mean and the shaded regions correspond to 95% confidence interval over 5 runs.